www.sciencemag.org/cgi/content/full/1176945/DC1

Supporting Online Material for

RNAi in Budding Yeast

Ines A. Drinnenberg, David E. Weinberg, Kathleen T. Xie, Jeffrey P. Mower, Kenneth H. Wolfe, Gerald R. Fink, David P. Bartel*

*To whom correspondence should be addressed. E-mail: dbartel@wi.mit.edu

Published 10 September 2009 on *Science* Express
DOI: 10.1126/science.1176945

This PDF file includes

Other Supporting Online Material for this manuscript includes the following:
(available at www.sciencemag.org/cgi/content/full/1176945/DC1)

Table S5. Transcripts that overlap siRNA-producing loci.

Drinnenberg et al., *Science* 2009

Supporting Online Material

Materials and Methods

Growth conditions and genetic manipulations

S. castellii was grown at 25°C on standard *S. cerevisiae* plate and liquid media (e.g., YPD and SC). Transformations were performed as described (*S1*) with some modifications. Either 0.5–2 µg plasmid DNA or 1–7 µg linear DNA was added to 5 µl single-stranded DNA (10 mg/ml salmon sperm DNA, Sigma D7656), mixed with 50 µl yeast (~3 x 10^8 cells in 100 mM lithium acetate), and added to transformation buffer (a mixture of 240 µl 40% PEG 3350 and 36 µl 1 M lithium acetate). After incubation at 25°C for 30–90 min, 35 µl of DMSO was added, and the entire mixture was incubated at 42°C for 10 min, resuspended, and then plated on selective media.

Other species. Growth temperatures were as follows, unless otherwise noted: *K. polysporus*, 25°C; *S. cerevisiae*, *S. bayanus*, and *C. albicans*, 30°C; *E. coli*, 37°C.

Strain construction

A list of strains used and generated in this study is provided (table S7).

Heterothallic strains. Most of our strains started with the homothallic *S. castellii* strain Y235 (*ura3-1*/*ura3-1*, *Ho*/*Ho*), generously provided by M. Cohn (*ura3-1* is a point mutation G541A that creates the amino acid substitution G181R). To delete the Ho endonuclease, the loxP-KanMX6-loxP module of plasmid pUG6 (*S2*) was used as a template to amplify the disruption cassette by fusion PCR (*S3*), with ~400-bp targeting arms on both sides of the cassette (primers 5′-TGATCGAAGAAGGCACTAGAA and 5′-CAGATCCACTAGTGGCCTATGCGGCCGCTGTCATTGAAAATCGCCAAA, 5′-GCGTACGAAGCTTCAGCTGGCGGCCGCGGCCAAATTCTTCCTGCAACT and 5′-TTTTCGGACTTCACGAGCTT). The resulting heterozygous strain (*ura3-1*/*ura3-1*, *Ho*/*ho::loxP-KanMX-loxP*) was transformed with pSH47 (*S2*), which encodes the *Cre* recombinase under the control of the *S. cerevisiae GAL1* promoter. The expression of *Cre* was induced for 2 h in liquid culture, and strains sensitive to G418 were isolated. This strain was transferred to sporulation medium (1% potassium acetate, 0.1% yeast extract, 0.05% glucose) for 4 days, and tetrads were dissected. Although sporulation efficiency and spore viability were generally low in Y235, stable heterothallic strains of mating type **a** and α (DPB004 and DPB005, respectively) could be derived from a tetrad with four viable spores, showing that *S. castellii ho* deletion strains could not switch mating type.

Deletion of AGO1 *and* DCR1. *AGO1* and *DCR1* were deleted using the hygromycin cassette of pAG32 (*S4*) and the loxP-KanMX6-loxP cassette of pUG6 as dominant selection markers, respectively. For diploids, homozygous deletions (DPB002 and DPB003) were generated first by deleting one copy in Y235, sporulating the resulting heterozygotes, and allowing isolated spores to grow, switch mating types, and mate. *AGO1* and *DCR1* were deleted in DPB004 and DPB005 to generate DPB006, DPB007, DPB008, DPB009, and DPB313. The *AGO1* disruption construct was created as follows: *AGO1* was amplified from genomic DNA (5′-TGAACGTGTGGAAGACCAAA and

5′-AGTGGCTAACGGCAACATATCAGACA) and cloned into pCR4Blunt-TOPO (Invitrogen); the hygromycin cassette was then inserted between the *Hind*III and *Age*I restriction sites within the *AGO1* genomic fragment; the *AGO1* disruption construct was then amplified with the same primers used for *AGO1* cloning. Deletion of *DCR1* was analogous to deletion of *Ho* (fusion PCR primers 5′-TTCAACACCTCCAGCAACAG and 5′-CAGATCCACTAGTGGCCTATGCGGCCGCAGGCATTGCAACAATCTGTG, 5′-GCGTACGAAGCTTCAGCTGGCGGCCGCGCTGTTGCTGGAGGTGTTGAA and 5′-TTTACCACCATACCATGAGTTTTT).

Tagged Ago1 strain for immunoprecipitation. A haploid strain expressing $Flag_3$-tagged Ago1 from its native promoter (DPB220) was constructed by two-step homologous recombination in DPB005, as follows: a *S. cerevisiae URA3* expression cassette (amplified from pYES2.1, Invitrogen) was used to replace the start codon of *AGO1* by transformation and selection of transformants on SC–ura plates; the *URA3* cassette was subsequently replaced by a $Flag_3$ tag (amplified with a start codon from pQCXIP, gift of D. Sabatini) by transformation and selection on 5-FOA.

S. castellii *GFP reporter strains*. The loxP-KanMX6-loxP cassette in DPB009 was removed by *Cre* expression as described above to generate DPB318. The GFP(S65T)-KanMX6 module from pFA6a (*S5*) was then integrated at the endogenous *ura3* locus in DPB005, DPB313, and DPB318 (such that GFP was fused in-frame directly after the ATG start codon of *ura3*) to generate GFP-expressing strains DPB314, DPB317, and DPB321. The silencing constructs (pIp, pIp-weakSC_GFP, and pIp-strongSC_GFP) were integrated upstream of the ORF annotated as Scas_633.2 in DPB314, DPB317, and DPB321 to create strains DPB331–DPB339. For these integrations, each silencing construct was linearized by digestion with *Sac*I, and 1.5 µg was transformed. Transformants were selected on SC–ura plates.

S. cerevisiae *RNAi reporter strains*. The GFP(S65T)-KanMX6 module from pFA6a was integrated at the endogenous *ura3* locus in L4718 to create DPB249. Integration of Ago1 and Dcr1 expression vectors (pRS404-P_{TEF}-Ago1 and pRS405-P_{TEF}-Dcr1) and GFP silencing construct vectors (pRS403-P_{GAL1}-weakSC_GFP and pRS403-P_{GAL1}-strongSC_GFP) into the genome was done by linearization and transformation using standard protocols (*S6*) to create DPB250, DPB251, and DPB255–DPB260. To generate strains useful for *URA3* silencing, DPB249 and DPB258 were transformed with functional *URA3* coding sequence amplified from pRS406 to create the uracil prototrophs DPB271 and DPB275, respectively. Integration of the silencing construct pRS403-P_{GAL1}-hpSC_URA3 into DPB271 and DPB275 generated DPB272 and DPB276, respectively.

Plasmid construction

A list of plasmids generated in this study is provided (table S8).

Yeast Ago1 *and* Dcr1 *expression plasmids*. *S. castellii AGO1* or *DCR1* was cloned into pYES2.1 (Invitrogen) to produce the galactose-inducible Ago1 and Dcr1 expression plasmids pYES2.1-Ago1 and pYES2.1-Dcr1, respectively. *GFP* was also cloned into pYES2.1 (creating pYES2.1-GFP) as a negative control.

E. coli *recombinant expression plasmids*. For recombinant expression of Dcr1 in *E. coli*, *DCR1* was cloned into pET101/D-TOPO, creating pET101-Dcr1. pET101-lacZ was supplied by the manufacturer (Invitrogen).

S. castellii *GFP silencing constructs*. A multiple cloning site containing *Xho*I and *Eco*RI restriction sites was cloned between the *Pvu*II and *Xba*I restriction sites of pYES2.1. For the strong silencing construct, 275 bp of *GFP* sequence from pFA6a was then cloned in the sense orientation between *Pvu*II and *Xho*I sites, and in the antisense orientation between *Eco*RI and *Xba*I sites, in *E. coli* SURE (Stratagene). The weak silencing construct was made identically, except without *GFP* sequence in the antisense orientation. A 73-bp sequence spanning intron 1 from *S. pombe rad9* was then added between *Xho*I and *Eco*RI sites (modeled after (*S7*)). To convert these episomal plasmids into integrating plasmids, the 2-micron and f1 origins were then replaced (using *Nhe*I and *Spe*I sites) by sequence from *S. castellii* sc633:288301–289016 (amplified from genomic DNA with 5′-AAAAGCTAGCGATCCCTTATCAAATATGGTAC and 5′-AAAAACTAGTGTAGAATCCAGAGAATAGAATC). These resulting *S. castellii* integrating plasmids expressing weak and strong *GFP* silencing constructs are pIp-weakSC_GFP and pIp-strongSC_GFP, respectively. The pIp empty vector was created by replacing the hairpin of pIp-strongSC_GFP with *Xho*I and *Eag*I sites.

S. cerevisiae *reconstitution and silencing constructs*. Vectors pRS404-P_{TEF}-Ago1 and pRS405-P_{TEF}-Dcr1 were constructed by insertion of the coding sequence of the respective *S. castellii* genes between the *TEF* promoter and *CYC1* terminator (cloned from pRS416-P_{TEF} (*S8*)) of the appropriate vector (*S9*) using *Spe*I and *Xho*I sites (Ago1) or *Xba*I and *Xho*I sites (Dcr1). To generate vectors pRS403-P_{GAL1}-strongSC_GFP and pRS403-P_{GAL1}-weakSC_GFP, an expression cassette containing the *GAL1* promoter, *CYC1* terminator, and GFP silencing construct sequence was cloned out of the appropriate episomal pYES2.1 silencing construct into the *Not*I and *Sal*I sites of pRS403. To generate the *URA3* silencing vectors, 339 bp of *URA3* sequence from pRS406 was initially cloned into the episomal pYES2.1 GFP weak silencing construct in the sense orientation between *Pvu*II and *Xho*I sites (thereby replacing the *GFP* sequence), and in the antisense orientation between *Eco*RI and *Xba*I sites. pRS403-P_{GAL1}-hpSC_URA3 was then created by cloning an expression cassette containing the *GAL1* promoter, *CYC1* terminator, and *URA3* silencing construct sequence out of this pYES2.1 plasmid into the *Not*I and *Sal*I sites of pRS403.

In vitro dsRNase assays

Substrates. Blunt-ended dsRNA substrate was prepared by simultaneous *in vitro* transcription from two PCR templates carrying T7 promoter sequences at opposite ends. Reactions were assembled using the MAXIscript Kit (Ambion) with a 32:1 molar ratio of UTP:[α-^{32}P]UTP (800 Ci/mmol) according to the manufacturer's directions. Control ssRNA was prepared similarly, except that a single PCR template was included in the transcription reaction. DNase-treated RNA was fractionated on a 4% urea gel, eluted from gel slices in 0.3 M NaCl overnight at 4°C, and ethanol precipitated.

Strains. Wild-type strains used in Figure 2A were *S. castellii* Y235, *K. polysporus* KpolWT, *C. albicans* Can14, and *S. cerevisiae* FY45. Strains used in Figure 2E were as follows: *S. castellii*, DPB005, DPB318, and DPB318 transformed with pYES2.1-Dcr1; *S. cerevisiae*, F2005 and F2005 transformed with either pYES2.1-Dcr1 or pYES2.1-GFP; *E. coli*, BL21 Star(DE3) (Invitrogen) transformed with either pET101-lacZ or pET101-Dcr1.

Extracts. Strains in Figure 2A were grown in YPD to OD_{600} 1.2–1.6; yeast strains in Figure 2E were grown similarly, except P_{GAL1} strains were grown in SC–ura with galactose/raffinose, and all strains were grown at 25°C; *E. coli* were grown in LB with 100 µg/ml ampicillin to OD_{600} 0.6 and induced (1 mM IPTG) for 4 h. Cells were harvested by centrifugation and flash frozen in 100–200 mg aliquots. Aliquots were thawed on ice, resuspended in 1 µl/mg lysis buffer [50 mM HEPES pH 7.6, 5 mM $MgCl_2$, 0.1 mM EDTA, 0.1 mM EGTA, 300 mM sodium acetate, 5% glycerol, 0.25% NP-40, protease inhibitor cocktail (Roche), 1 mM PMSF], and vortexed four times for 45 s at 4°C with an equal volume of glass beads. Lysates were clarified by centrifugation at 10,000x *g* for 5 min. Extract concentrations were normalized according to absorbance at 260 nm and stored at –80°C.

Reactions. The 20 µl reactions contained 10 µl extract (or 10 µl lysis buffer for "Buffer only" control), 4 µl 5X reaction buffer (125 mM HEPES pH 7.2, 10 mM magnesium acetate, 10 mM DTT, 5 mM ATP), and 10,000 cpm radiolabeled substrate. In Figure 2A, reactions were incubated at 25°C (*S. castellii* and *K. polysporus*) or 30°C (all others) for 2 h; in Figure 2E all reactions were incubated at 25°C. Reactions were quenched with AE Buffer (50 mM sodium acetate pH 5.5, 10 mM EDTA) and phenol extracted.

RNA blots

Total RNA was isolated using the hot phenol method. Small RNA blots were performed using 10–15 µg total RNA per lane and carbodiimide-mediated cross-linking to the membrane (*S10*), with the following DNA probes radiolabeled at their 5′ termini: *S. castellii* siRNA sc1056, 5′-CTATCTTCATCGATTACCATCTA; *S. castellii* U6 small nuclear RNA, 5′-TATGCAGGGGAACTGCTGAT; *GFP* siRNA, 5′-ACCATTATCAACAAAATACTCCAATTGGCGATGGCCCTGTCCTTTTACCA; Ty1 probe 1, 5′-CCGTTAGACGTTTCAGCTTCCAAAACAGAAGAATGTGAGAAGGCTTCCACTAAG; Ty1 probe 2, 5′-TAAATTAGTGGAAGCTGAAACGCAAGGATTGATAATGTAATAGGATCAATGAATATAAAC. mRNA blots were performed using 4–5 µg DNase-treated total RNA per lane and UV crosslinking. *GFP* and Ty1 body-labeled antisense riboprobes were prepared by using PCR products as templates for in vitro transcription (MaxiScript kit, Ambion). A radiolabeled *PYK1* (*CDC19*) DNA probe was prepared by random priming (Prime-It II, Stratagene).

Strains used in Figure 2B were Y235, DPB002, DPB002 transformed with pYES2.1-Ago1, DPB003, and DPB003 transformed with pYES2.1-Dcr1. Strains used in Figure 4B were DPB331–DPB339. Strains used in Figure 4D and 4F were DPB249–DPB251, and DPB255–DPB260. Strains used in Figure 5D were DPB249, DPB255, and DPB258.

RT-PCR

Reverse transcription reactions were performed with 100 ng total RNA using Superscript III according to the manufacturer's instructions (Invitrogen) with the following gene-specific primers in the same reaction: *GFP*, 5′-TGTGGTCTCTCTTTTCGTTGG; *ACT1*, 5′-TCAAAGAAGCCAAGATAGAACCA. PCR reactions were assembled in 100 µl with 2 µl RT reaction using the following primers: *GFP*, 5′-TTTCACTGGAGTTGTCCCAAT and 5′-GAAAGGGCAGATTGTGTGG; *ACT1*, 5′-ACGTTGGTGATGAAGCTCAA and 5′-ATACCTGGGAACATGGTGGT. After the indicated number

of cycles, a 15 µl aliquot was removed and combined with 3 µl 6X DNA loading dye. 6 µl was loaded onto a 1.5% agarose gel, and DNA was visualized by EtBr staining.

Plasmid loss

DPB005, DPB313, and DPB008 were transformed with 1.5 µg pRS316 (*S8*), pYES2.1-weakSC_GFP, pYES2.1-Ago1, or pYES2.1-Dcr1. Transformants were plated directly on SC–ura plates containing 2% glucose (uninduced) or 2% galactose (induced). To analyze plasmid loss, cells from colonies were inoculated in 5 ml of the medium indicated in Figure S11 and passaged once a day for 4 days.

Southern blots

Each lane contained 2 µg of RNA-free DNA isolated as described in (*S11*) and digested with *Xba*I. Plasmids were detected using a probe with the ampicillin-resistance gene sequence (amplified using primers 5′-CCATGAGTGATAACACTGCG and 5′-GGCACCTATCTCAGCGATC). The genomic locus was detected using a probe with sequence from *S. castellii* sc718:138001–138427 (amplified using primers 5′-GCATAAGCTGTGCTTTAGACT and 5′-CTTGTAACGGTTCAATTCTAGC).

FACS analysis

Two biological replicates of each strain were inoculated in SC, either noninducing (2% glucose) or inducing (*S. castellii*, 2% galactose; *S. cerevisiae*, 1% galactose and 1% raffinose), and grown overnight. Fresh cultures were then seeded from the overnight cultures and cells were grown to log-phase. Cells were analyzed using FACSCalibur (BD Biosciences); data were processed with CellQuest Pro (BD Biosciences) and FlowJo (Tree Star). The same samples were used for RNA and GFP analyses.

***S. cerevisiae URA3* silencing**

Strains (DPB249, DPB271–DPB272, DPB258, DPB275–DPB276) were inoculated in SC under inducing conditions (1% galactose and 1% raffinose) and grown for 1 day. Cells were diluted to OD_{600} of 1.0, and 1:10 serial dilutions were spotted onto the appropriate plates (SC, SC–ura, or 5-FOA; all containing 1% galactose and 1% raffinose) and grown at 30°C for 3 days.

***S. cerevisiae* Ty1 analysis**

Transposition assay. Strains (DPB249, DPB255, and DPB258) were transformed with 1 µg of pGTy*H3HIS3* (galactose-inducible Ty1 marked with *HIS3*, where transcription of the Ty1 and *HIS3* is in the same direction) (*S12*) and selected on SC–ura plates. Transformants were streaked out on SC–ura with 2% galactose plates and grown at 20°C for 2 days to induce transposition. Cells were then replica-plated onto YPD plates and grown at 30°C for 1 day for plasmid loss. These cells were then replica-plated onto 5-FOA–his plates (to select for both plasmid loss and transposition) or 5-FOA plates (to select for plasmid loss only) and grown at 30°C for 2–3 days.

When using the more standard *his3*-artificial-intron marker for retrotransposition (*S13*), analogous results were obtained but were not as informative because the marker produces a non-physiological antisense transcript, which could pair with the sense transcript to generate an ectopic dsRNA trigger.

RNA and protein analysis. Strains (DPB249, DPB255, and DPB258) were inoculated in SC and grown overnight. For non-transposition-inducing conditions, cells were diluted to OD 0.125 and grown at 30°C to OD_{600} 0.9–1.0. For transposition-inducing conditions, cells were diluted to 100 cells/ml and grown at 20°C to OD_{600} 0.9–1.0. Cells were harvested by centrifugation and flash frozen.

Immunoblotting. Three OD_{600} units of cells were resuspended in 100 ml H_2O. After adding 160 µl of extraction buffer (1.85 M NaOH, 7.4% β-mercaptoethanol), cells were incubated on ice for 10 min. 160 µl of 50% trichloroacetic acid was added, and cells were incubated on ice for an additional 10 min. Precipitated material was collected by centrifugation, and the supernatant was discarded. The tube was washed with 500 µl of 1 M Tris pH 8.0, centrifuged briefly, and the supernatant was discarded. The pellet was vigorously resuspended in 150 µl of 1X Laemlli sample buffer and boiled for 4 min. Samples (12 µl each) were resolved by SDS-PAGE, transferred to poly(vinylidene difluoride) in CAPS-ethanol pH 10, and probed sequentially with Ty1-VLP antiserum (*S14, 15*) and anti-actin (Abcam, ab8224). Immunoblots were developed with HRP-conjugated anti-rabbit or anti-mouse antibodies and enhanced chemiluminescence (Amersham).

Small-RNA sequencing and analysis

Library preparation. Total RNA was isolated using hot phenol from log-phase YPD cultures of *S. castellii* F2037, *K. polysporus* KpolWT, *S. cerevisiae* FY45, *S. bayanus* F2035, and *C. albicans* Can14. Small-RNA cDNA libraries were prepared as described (*S16*) and sequenced using the Illumina SBS platform. Libraries were also prepared and sequenced from RNAi deletion strains (DPB002 and DPB003).

Ago1 immunoprecipitation. A saturated overnight culture of DPB249 was diluted to OD_{600} 0.3 in 150 ml YPD and grown to OD_{600} 1.5. Extracts were prepared as for *in vitro* dsRNase assays. For the input fraction, one-fifth of the extract was removed and added to AE buffer. Anti-Flag M2 agarose (Sigma) was incubated with the remaining extract at 4°C for 1.5 h. Beads were washed with lysis buffer four times, after which the remaining buffer was removed and AE buffer was added. Small RNA libraries were prepared as described above.

Read processing. After removing the adaptor sequences, reads representing the small RNAs were collapsed to a non-redundant set, and 14–30-nt sequences were mapped to the appropriate genome, allowing no mismatches and recovering all hits (table S1). When counting the reads matching a locus, the count was hit-normalized, i.e., normalized to the number of times that a small-RNA sequence matched the genome. For example, a small RNA sequenced twice that mapped to the genome five times contributed 0.4 read counts to each genomic locus. Sequence and feature files for *S. cerevisiae* S288C and *C. albicans* SC5314 were obtained from the *Saccharomyces* Genome Database (SGD) on September 10, 2007 and the *Candida* Genome Database Assembly 21. Sequence files for *S. bayanus* MCYC623 that were current as of January 18, 2009 were downloaded from NCBI. Sequence and feature files for *S. castellii* CBS4309 and

K. polysporus DSM70294 were obtained from the Yeast Gene Order Browser (YGOB) (*S17*). Using the set of *S. cerevisiae* tRNA and rRNA sequences as queries for blastn alignments (e-value cutoff, e-10), genomic loci mapping to tRNA and rRNA in *S. castellii*, *K. polysporus*, and *S. bayanus* were identified. In *K. polysporus*, tRNA and rRNA annotations were available in the GenBank flatfile obtained from YGOB and used to supplement the alignments.

Initial identification of siRNA clusters. For the small RNAs sequenced from total RNA, genomic regions giving rise to siRNAs were identified by parsing the genome files from *S. castellii*, *K. polysporus*, and *C. albicans* into non-overlapping windows of 500 bp. Windows with high levels of siRNA expression (22–23-nt sequences for *S. castellii* and *K. polysporus*, 21–22-nt sequences for *C. albicans*; excluding tRNA and rRNA reads) were selected by applying read and sequence density cutoffs manually adjusted based on the data set (*S. castellii*, ≥10 reads/kb or ≥10 genome matches/kb; *K. polysporus*, ≥50 reads/kb or ≥50 genome matches/kb; *C. albicans*, ≥40 reads/kb or ≥40 genome matches/kb). Adjacent windows passing the density cutoffs were concatenated. The small-RNA profile of each of these clusters was manually inspected for adherence to properties, including length (23 nt for *S. castellii* and *K. polysporus*; 22 nt for *C. albicans*) and 5′-nt biases (U for *S. castellii* and *K. polysporus*; A or U for *C. albicans*).

Refined identification of siRNA clusters in S. castellii. Using sequencing reads of small RNAs co-purifying with Ago1, a hidden Markov model (HMM) was constructed with two states, "C" (giving rise to siRNAs) and "N" (not giving rise to siRNAs). The ratio of 23-mer reads relative to all reads (excluding 22-mer reads) was calculated in 10-bp windows (apportioning hit-normalized counts to the windows based on the fraction of its nucleotides covered by the small RNA) to define two types of emissions: 0) ratio ≥0.45 and 1) ratio <0.45. Emission probabilities were generated by training on the initially identified siRNA clusters to represent the "C" state, and training on five supercontigs (sc1014, sc621, sc542, sc534 and sc587) to represent the "N" state. Transition probabilities for the given window size were estimated using the median length of these siRNA clusters (250 bp) that map to Y′ elements and palindromic arms, or the average length of the intervening genomic sequence between two clusters, i.e. the difference derived from the total length of all contigs (11,354,548 bp) divided by the number of clusters identified in the initial analysis (100). Initial state probabilities were calculated based on the proportion of contigs in "C" state, i.e. total length of siRNA clusters (25,000 bp) divided by the total length of all contigs. Using the Viterbi algorithm, the contigs were parsed over non-overlapping 10-bp windows. The parse yielded 379 clusters (table S3) with the three regions that map to rRNA excluded. The cluster boundaries were adjusted to include the full sequence of all small RNAs with at least one nucleotide mapping to the cluster and to exclude terminal nucleotides not covered by a small RNA.

Cluster annotation. Clusters were further characterized based on previous genome annotations and alignments. Reads for Figure 1C (21–23 nt) and for figure S3 (22–23 nt) were classified into categories. Reads of siRNA clusters that mapped to annotated ORFs in either sense or antisense orientation were grouped together in Figure 1C as reads from ORF clusters. Using the $Flag_3$-Ago1 IP dataset, siRNA reads in clusters overlapping ORFs were further separated into "clusters sense to ORF" and "clusters antisense to ORF." siRNA reads that mapped to convergent overlapping ORF transcripts (annotated using the mRNA-Seq dataset) were categorized as "overlap."

The DNA sequences of the siRNA clusters from the *S. castellii* and *K. polysporus* datasets were aligned against the *S. cerevisiae* protein dataset (NCBI) using blastx (e-value cutoff 0.001). Significant alignments to Ty elements were extended 300 nt on both sides, and reads overlapping these extended alignments were classified as Ty-proximal siRNA reads. Additional Ty elements could be identified using annotated Ty elements from (*S18*) as blastx queries. More careful Ty annotations for *S. castellii* could then be made by identifying *S. castellii* Ty LTR, gag, and pol sequences based on the initial blastx matches and other Ty sequence signatures ((*S18-20*) and references therein). Similarly, siRNA clusters derived from Y′ elements were detected. For cases in which siRNA expression exceeded the boundaries of the annotated Y′ element ORF in a processive, un-gapped fashion, those siRNAs were still classified as Y′-element-proximal siRNAs. siRNA clusters in *C. albicans* were annotated based on the *C. albicans* genome annotation and blastx alignments against the set of protein sequences downloaded from NCBI (e-value cutoff 0.001).

Palindromes were predicted using the IRF program (*S21*) with the following parameters: Alignment Parameters, 2, 3, and 5 (match, mismatch, and indels, respectively); minimum Alignment Score To Report Repeat, 100; T4 small palindromes (20–80+ nt) loop length, 100 nt; T5 medium palindromes (80–300+ nt) loop length, 1000 nt; T7 large palindromes (300–2400+ nt) loop length, 5000 nt; maximal loop length, 5000 nt; maximal stem length, 10,000 nt; allow GT matches. The following numbers of palindromes were identified: 66 in *S. castellii*, 222 in *K. polysporus*, 61 in *C. albicans*, and 390 in *S. cerevisiae*. These palindromes were compared to our lists of siRNA-generating loci. In most cases when overlap was observed, the 22–23-nt RNAs were enriched in the inverted-repeat regions rather than the intervening region or surrounding regions. In some cases the palindromes overlapped with each other and the one with 22–23-nt RNAs mapping to the repeats was the one chosen. In some cases (10 of 43 for *S. castellii*, and 42 of 90 for *K. polysporus*), the overlap of 22–23-nt RNAs was not preferentially at the repeats; these were not classified as palindromic clusters. Using the initial datasets, these analyses revealed 19 palindromic siRNA clusters in *S. castellii* and 29 in *K. polysporus*, all of which either overlapped or were contained within the set of siRNA clusters identified by the sliding window approach. The refined cluster identification based on the $Flag_3$-Ago1 IP dataset from *S. castellii* revealed 23 palindromic siRNA clusters (table S5).

Phasing analysis. The frequency of distances separating all 23-mer 5′-end pairs (i, j) mapping to the same DNA strand was calculated using the following equation:

$$Frequency_D = \sum_{i,j} (Reads_i \cdot Reads_j)_D$$

where D = distance between sRNA 5′ ends

The frequency of distances separating pairs of 23-mer 5′ ends mapping to opposite strands of DNA was calculated separately using the same equation.

Phylogenetic analysis

Psi symbols for *S. pastorianus* (Fig. 1A) indicate a highly degraded *AGO1* pseudogene and a *DCR1* pseudogene that is intact except for a single internal stop codon. The intact *S. bayanus DCR1* gene shows conservation of amino acid sequence relative to the *S. pastorianus*

pseudogene (*dN*/*dS* ratio 0.3) despite the absence of intact *AGO1* in both species. The *AGO1* and *DCR1* loci are syntenic among *S. castellii*, *K. polysporus*, *S. pastorianus,* and *S. bayanus*.

A maximum-likelihood (ML) tree of RNaseIII domains was constructed using the PHYLIP software package (http://evolution.genetics.washington.edu/phylip.html). RNaseIII domains were predicted using SMART (*S22, 23*). The amino acid sequences of the RNaseIII domains were used to compute a multiple sequence alignment using TCOFFEE (*S24*). A consensus ML tree was built by running DNAML (PHYLIP) on the amino acid alignment after bootstrap re-sampling (500 replicates) of the data set using SEQBOOT (PHYLIP). The phylogenetic tree was displayed using TreeView (http://taxonomy.zoology.gla.ac.uk/rod/treeview.html).

Protein name/accession numbers used in Figure 2D are as follows: At1, *A. thalania* DCL1; At2, *A. thalania* DCL2; Ca1, *C. albicans* EAK98282; Ca2, *C. albicans* XP_717277; Ct1, *C. tropicalis* AAFN01000070; Ct2, *C. tropicalis* AAFN01000057; Cn1, *C. neoformans* XP_569593.1; Cn2, *C. neoformans* XP_569797.1; Dh1, *D. hansenii* XP_457483.1; Dh2, *D. hansenii* XP_457193.1; Hs, *H. sapiens* DICER1; Kl, *K. lactis* F2416; Kp1, *K. polysporus* 1045p1; Kp2, *K. polysporus* 455p11; Mg1, *M. grisiae* XP_363615; Mg2, *M. grisiae* XP_367242; Mg3, *M. grisiae* XP_367242; Nc1, *N. crassa* Sms3; Nc2, *N. crassa* Dcl2; Nc3, *N. crassa* NCU01762; Sb1, *S. bayanus* 671p65; Sb2, *S. bayanus* 643p2; Sca1, *S. castellii* 696p6; Sca2, *S. castellii* 626p5; Sc, *S. cerevisiae* Rnt1; Sp1, *S. pombe* Pac1; Sp2, *S. pombe* Dcr1.

To search for a PAZ domain in the *S. pombe* Dcr1 protein, the full-length protein sequence was submitted as a query to the HHpred server, allowing 10 PSI-BLAST iterations and 1000 maximum hits (*S25*). All available standard HMM databases (pdb70_3Sep09, pdb_on_hold_3Sep09, scop70_1.71, scop70_1.75, cdd_17Jul09, interpro_16.2, pfamA_23.0, smart_17Jul09, panther_4Mar08, tigrfam_4Mar08, pirsf_4Mar08, COG_17Jul09, KOG_17Jul09, CATH_4Mar08, supfam_4Mar08, pfam_17Jul09, cd_17Jul09, test56, test18) were searched, and the results realigned with the Maximum ACcuracy (MAC) alignment algorithm. The search retrieved a family that included full-length Dicers (KOG id: KOG0701; E-value = 0) and a crystallized Dicer derived from *Giardia intestinalis* (PDB id: 2qvw/2ffl; E-value = 1.1e-15), which both aligned to the *S. pombe* Dcr1 in regions that included their PAZ domains. The search also retrieved known PAZ-domain entries (CDD ids: cd02843, cd02844, cd02845, KOG id: KOG1042, Pfam id: PF02170; E-values = 7.9e-05, 2.3e-05, 0.95, 19, 0.018, respectively), even though these entries lacked flanking domains to aid in the alignment. The same procedure was performed replacing the full-length Dcr1 query with a region between the first dsRNA-binding domain and the first RNaseIII domain (a.a. 628–914 of the *S. pombe* Dcr1 protein), which encompassed the putative PAZ region but no other known domains. This search also retrieved Dicer proteins and other known PAZ domain entries. Analogous searches did not provide evidence for a PAZ domain in *S. castelli* Dcr1p.

mRNA sequencing and analysis

Strand-specific mRNA-Seq. Two biological replicates of DPB005 (WT), DPB007 (Δ*ago1*), and DPB009 (Δ*dcr1*) were grown in YPD to OD_{600} 0.6–0.8. Total RNA isolated using hot phenol was treated with DNaseI (RiboPure-Yeast Kit, Ambion). Poly-$(A)^+$ mRNA was purified from 75 µg total RNA using magnetic oligo-dT DynaBeads (Invitrogen) according to the manufacturer's instructions, and then fragmented by alkaline hydrolysis (*S26*). Trace amounts of synthetic 3′-

pCp[5′-^{32}P]-labeled 26-nt and 32-nt RNA size markers were added to monitor the subsequent steps. RNA fragments (25–45 nt) were gel-purified and 3′-dephosphorylated in a 25 µl reaction containing 12.5 units T4 PNK (New England Biolabs) and MES-NaOH buffer (100 mM MES-NaOH pH 5.5, 10 mM $MgCl_2$, 10 mM β-mercaptoethanol, 300 mM NaCl) for 6 h at 37°C. After phenol extraction and precipitation, RNA was ligated to pre-adenylated adaptor DNA as described (*S16*). Gel-purified ligation products were 5′-phosphorylated in a 14 µl reaction containing 15 units T4 PNK and PNK buffer for 30 min at 37°C. After phenol extraction and precipitation, RNA was ligated to a 5′-adaptor RNA, gel-purified, converted to cDNA, amplified, and sequenced as described (*S16*).

Read processing. The first 25 nt of each 36-nt read were isolated and collapsed into a non-redundant set of 25-nt sequences with occurrence counts (table S4). Sequences were mapped to the reference genome, allowing no mismatches and recovering all hits. Transcript-specific analysis of small-RNA data (e.g., Fig. 3A) was based on 22–23-nt reads from the $Flag_3$-Ago1 IP dataset, unless indicated otherwise.

Exon annotations were downloaded from YGOB (introns less than 10 nt were considered sequencing errors and assigned as exons). Sense mRNA, antisense mRNA, and antisense small-RNA read counts were calculated individually for each gene by summing the hit-normalized reads mapping either to the 5′-half of the ORF (mRNA tags, half-ORF analysis) or across all of the ORF (small-RNA reads); a sequence contributed $N \cdot nt/25$ reads to a gene (N = hit-normalized read number; nt = number of nt in the 25-nt sequence overlapping the ORF). In parallel, mRNA tag counts were also calculated across the entire ORF (full-ORF analysis, fig. S4).

For each gene, mRNA-Seq tag counts from biological replicates were averaged. Genes for which none of the three strains had an average tag count above 20 (half-ORF analysis) or above 30 (full-ORF analysis), and ORFs corresponding to Y′ element fragments, were excluded from all analyses except in figures S4A and S4B. mRNA abundance was calculated by dividing tag counts by kb of mapped exon. mRNA-Seq tag counts from Δ*ago1* were normalized to those of WT by first ranking genes based on the ratio of tags in Δ*ago1* versus WT, and then multiplying the WT tag counts by a factor such that the median ranked gene had a transcript abundance ratio of 1. An analogous normalization procedure was also applied to Δ*dcr1*. The final normalization factors were 0.8847 for WT, 1.0000 for Δ*ago1*, and 0.8440 for Δ*dcr1*. The same normalization factors were applied to the single-nucleotide-resolution mRNA-Seq plots for the Y′ element consensus (Fig. 3B).

Consensus Y′ element of S. castellii. An initial set of Y′-element fragments was obtained by extending and combining annotated Y′-element ORFs and Y′-element fragments manually identified in the course of annotating siRNA clusters. These fragments were assembled into a single contig using SeqMan Pro (DNASTAR Lasergene). The resulting majority sequence was used as a query for blastn against the genome (e-value cutoff 10^{-10}, MegaBlast option). All additional Y′ element fragments obtained from this search were added to the consensus, bringing to 32 the total number of unique contributing genomic fragments (fig. S5). mRNA tags and small-RNA reads were mapped to the consensus Y′ element independently of the genome. Each library was initially mapped to the set of Y′ element fragments, allowing no mismatches and recovering all hits. Mapped nucleotide positions with respect to fragments were converted into positions with respect to the consensus. Mapping data was normalized using the above factors and used to generate single-nucleotide-resolution plots of the consensus Y′ element (Fig. 3B).

Y′ element transcript and siRNA abundances were the sum of read and tag nucleotides across the region of interest divided by the appropriate length (25 nt for mRNA; 22 or 23 nt for siRNA).

Comparing ORF-derived siRNA levels with transcript levels. For each annotated protein-coding gene, mRNA tags and small-RNA reads mapping across its ORF were determined as above, except only uniquely mapping sequences were included. For each ORF, sense and antisense transcript abundances were estimated separately as the sum of tags from all six mRNA-Seq libraries (without normalization), and siRNA abundance was estimated as the sum of sense and antisense small-RNA reads. Genes with no unique mRNA-Seq tags mapping to the coding strand were excluded. Genes were ranked by total transcript abundance (sum of sense and antisense tags) and by inferred duplex abundance (minimum of sense and antisense tags). Genes with non-zero abundance were divided into three equally sized bins (high, mid, low). For inferred duplex analysis, genes with zero inferred duplex abundance (i.e., genes with sense tags but no antisense tags) formed a fourth bin.

Transcripts corresponding to siRNA-generating loci. For each siRNA cluster identified using the HMM, two transcripts—one on each strand—were initiated and assigned the coordinates of the cluster. Tags from Δ*dcr1* mRNA-Seq libraries were used to extend cluster transcripts as follows. The transcript was extended 10 nt in the 5′ direction if that 10-nt window had a tag density within 10-fold (above or below) of that of the initially assigned transcript. This process was iterated using the average tag density of the extended transcript. Once a window failing this criterion was reached, the transcript was terminated before the window. Then, the 3′ end was also thus extended, beginning with the average tag density of the transcript that included the extended 5′ end. Transcript extension was also tried first in the 3′ then in the 5′ direction; when the transcript ends disagreed between these two orders, the combination of 5′ and 3′ ends forming the largest transcript was used. The ends were then more finely mapped by identifying the first nucleotide upstream and last nucleotide downstream that corresponded to any tags (in Δ*dcr1* mRNA-Seq libraries), with a maximum extension of 10 additional nucleotides. Coordinates of inferred transcripts are presented in table S3. Transcripts that had mRNA-Seq tags mapping to them but that did not overlap any previous annotations were annotated as *non-coding-siRNA-generating* genes (*NCS*, table S3).

Transcript abundance in each mRNA-Seq library and siRNA abundance were determined as with coding transcripts, with the following exceptions: intron annotations were ignored, and an average read cutoff of 15 tags (half-transcript analysis) or 20 tags (full-transcript analysis) in any strain was applied. Y′-element fragments were removed and replaced with the consensus, except in table S3.

Protein-coding transcript extension and overlap. Of 5693 annotated ORFs, 5297 (93%) had mRNA-Seq tags mapping to at least 70% of the ORF nucleotides (combining tags from all three strains) and were carried forward for further analysis. For each ORF, the 5′ and 3′ boundaries of the transcript were extended using the mRNA-Seq tags, requiring contiguous tag coverage outward from the ORF boundaries and assigning the revised 5′ and 3′ boundaries to the most distal nucleotides represented by these mRNA-Seq tags.

A gene pair was defined as a gene and its right neighbor (according to YGOB annotations). The 5297 ORFs were parsed into 4776 gene pairs, with the loss of pairs attributable mainly to genes located at the ends of contigs. The number of convergent overlapping transcripts giving rise to *DCR1*-dependent siRNAs was calculated comparing 22–23-nt reads from the $Flag_3$-Ago1 input

and Δ*dcr1* datasets. 467 convergent overlapping loci had uniquely mapping small RNA reads in the $Flag_3$-Ago1 input dataset. The Δ*dcr1* dataset was then used to adjust this number to account for the loci for which small RNAs represented *DCR1*-independent mRNA degradation intermediates. Because RNA degradation intermediates would be overrepresented in the Δ*dcr1* small RNA dataset due to the absence of siRNAs, the Δ*dcr1* dataset was normalized to the $Flag_3$-Ago1 input dataset based on the number of rRNA and tRNA reads. Three normalized Δ*dcr1* datasets were constructed from the complete dataset by random sampling without replacement. In these three datasets, a median of 30 convergent overlapping loci had uniquely mapping Δ*dcr1* small RNA reads, which indicated that at least 437 convergent overlapping loci (43%) gave rise to *DCR1*-dependent uniquely mapping siRNAs.

To compare overlapping transcripts between *S. castellii* and *S. cerevisiae*, a list of gene pairs with opposite and overlapping transcripts in *S. cerevisiae* was downloaded from http://www.yale.edu/snyder/ (*S27*). The genes comprising these 828 unique gene pairs were mapped to their corresponding *S. castellii* genes based on YGOB annotations. 398 pairs corresponded to annotated convergent gene pairs in *S. castellii*. These pairs were cross-referenced with the list of *S. castellii* overlapping convergent gene pairs to determine the number producing overlapping transcripts in both species. Of the convergent gene pairs syntenic between these two genomes and reported to generate overlapping mRNAs in *S. cerevisiae* (*S27*), 84% generated overlapping mRNAs in *S. castellii*.

S. cerevisiae *mRNA-Seq analysis.* Strand-specific mRNA-Seq data from *S. cerevisiae* (*S26*) was downloaded from the Gene Expression Omnibus (samples GSM346117 and GSM346118) and processed as for *S. castellii*. Telomere annotations (TEL16L, TEL16R, TEL12L, and TEL12R) were downloaded from SGD, and hit-normalized tag counts were used to plot the abundance of mRNA-Seq tags at single-nucleotide resolution (i.e. tags contributed to counts along their entire length). To analyze mRNA-Seq tags mapping to a consensus Ty1 element, the 28 full-length Ty1 elements in the S288C genome sequence (identified using Ty1*H3* as a query for blastn against the genome) were aligned using SeqMan Pro (DNASTAR Lasergene). mRNA-Seq tags matching the consensus element were analyzed as for the consensus Y′ element of *S. castellii*, except tag counts were divided by 28 to obtain the average number of tags per full-length element at each position.

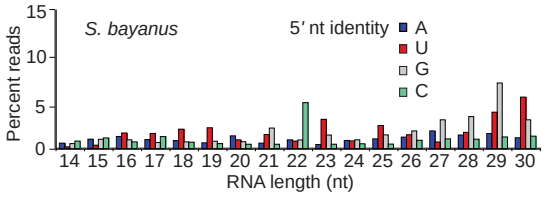

Figure S1. Analysis of small-RNA library from *S. bayanus* MCYC623. Length distribution of genome-matching reads (as percent of reads that do not match tRNA or rRNA) representing small RNAs with the indicated 5′ nucleotide (nt). Reads matching tRNAs and rRNAs were excluded.

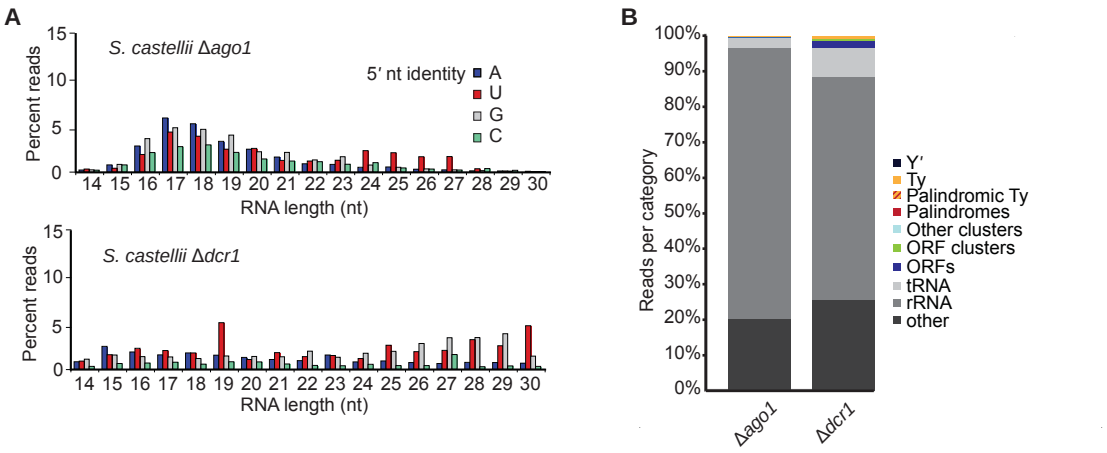

Figure S2. Analysis of small-RNA libraries from RNAi-mutant strains. **(A)** Length distributions of genome-matching reads (as percent of reads that do not match tRNA or rRNA) representing small RNAs with the indicated 5′ nucleotide (nt). Reads matching tRNAs and rRNAs were excluded.
(B) Classification of 21–23-nt reads based on genome annotations and alignments.

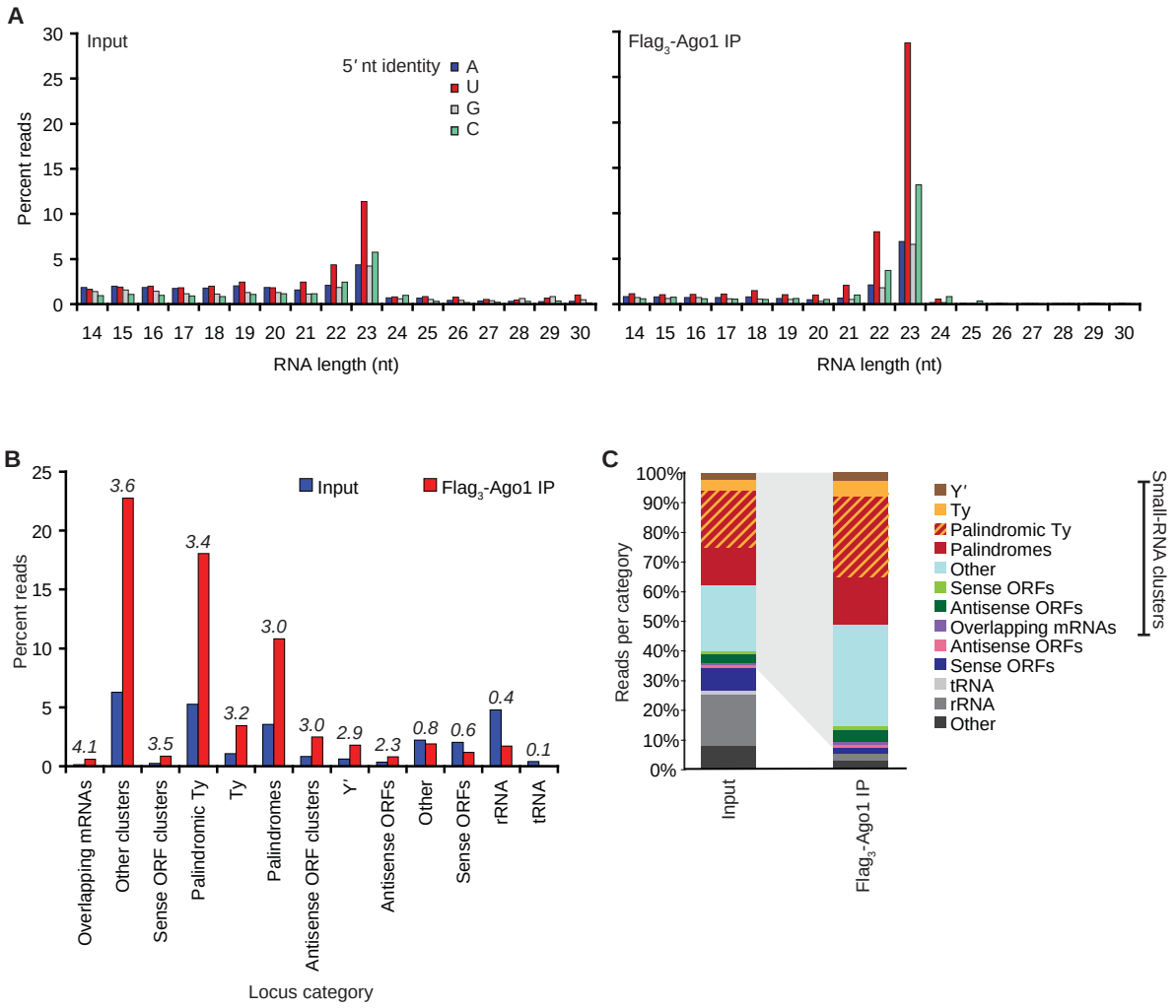

Figure S3. Sequencing of Ago1-associated small RNAs. **(A)** Length distribution of genome-matching sequencing reads representing small RNAs with the indicated 5′ nucleotide. Reads matching rRNA and tRNA are excluded. **(B)** Enrichment analysis of 22–23-nt reads based on genome annotation and alignments of their mapped loci. Italicized numbers above bars represent fold-enrichment calculated as (% of total reads in IP)/(% of total reads in Input). **(C)** Classification of 22–23-nt reads based on genome annotation and alignments of their mapped loci, considering those that map to clusters in a pattern suggestive of siRNAs separately from those that do not. Gray shading indicates the fraction of small RNAs considered to be siRNAs.

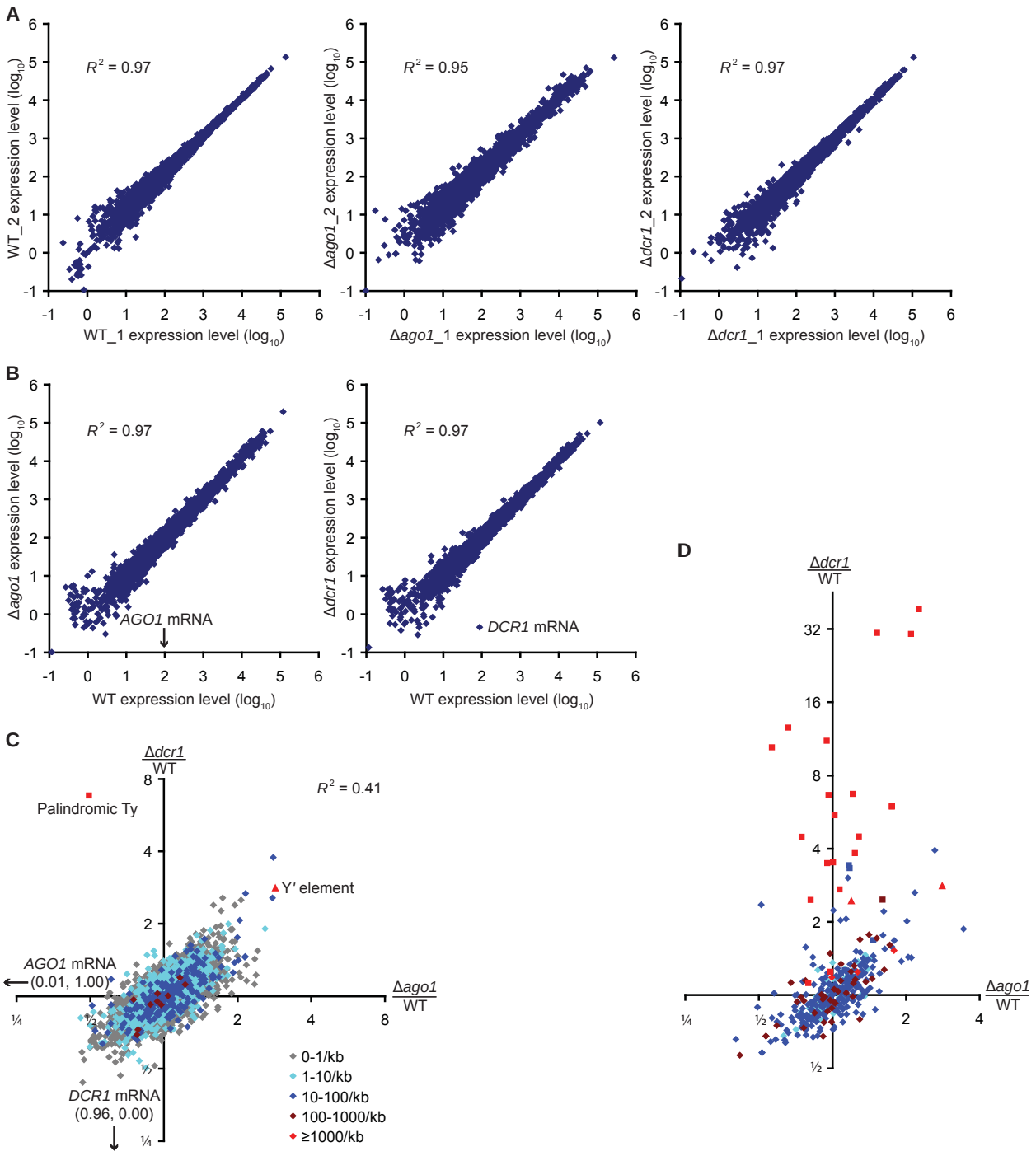

Figure S4. mRNA-Seq analysis of wild-type and RNAi-mutant strains. **(A)** Correlation in transcript abundance between biological replicates. The number of tags mapping to the 5′ half of each annotated ORF was used to estimate the abundance of full-length transcripts. Expression level was calculated as tags per kilobase of coding exon. **(B)** Correlation in transcript abundance between wild-type and RNAi-mutant strains. Plots are as in (A). *AGO1* mRNA had 96.77 tags/kb and 0 tags/kb in WT and Δ*ago1* strains, respectively. **(C)** Plot is as in Figure 3A, except that transcript abundance was calculated using tags across the entire ORF. **(D)** Plot is as in Figure 3C, except that transcript abundance was calculated using tags across the entire transcript.

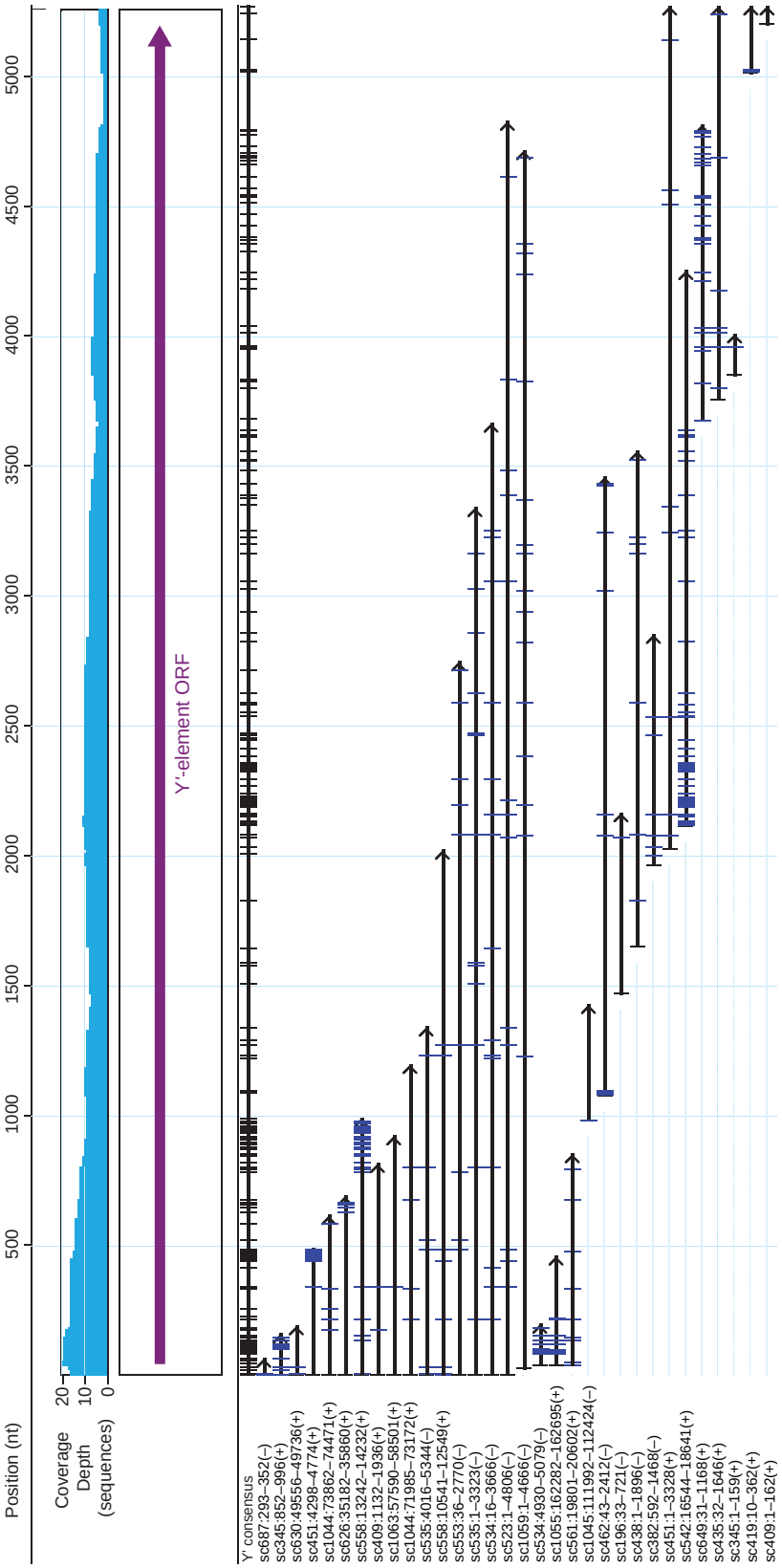

Figure S5. Assembly of a *S. castellii* Y′-element consensus sequence. Y′-element fragments were assembled into a single consensus sequence as described in Materials and Methods. Vertical bars represent single-nucleotide polymorphisms with respect to the majority sequence, many of which fell at the ends of contigs and are presumed to include sequencing errors.

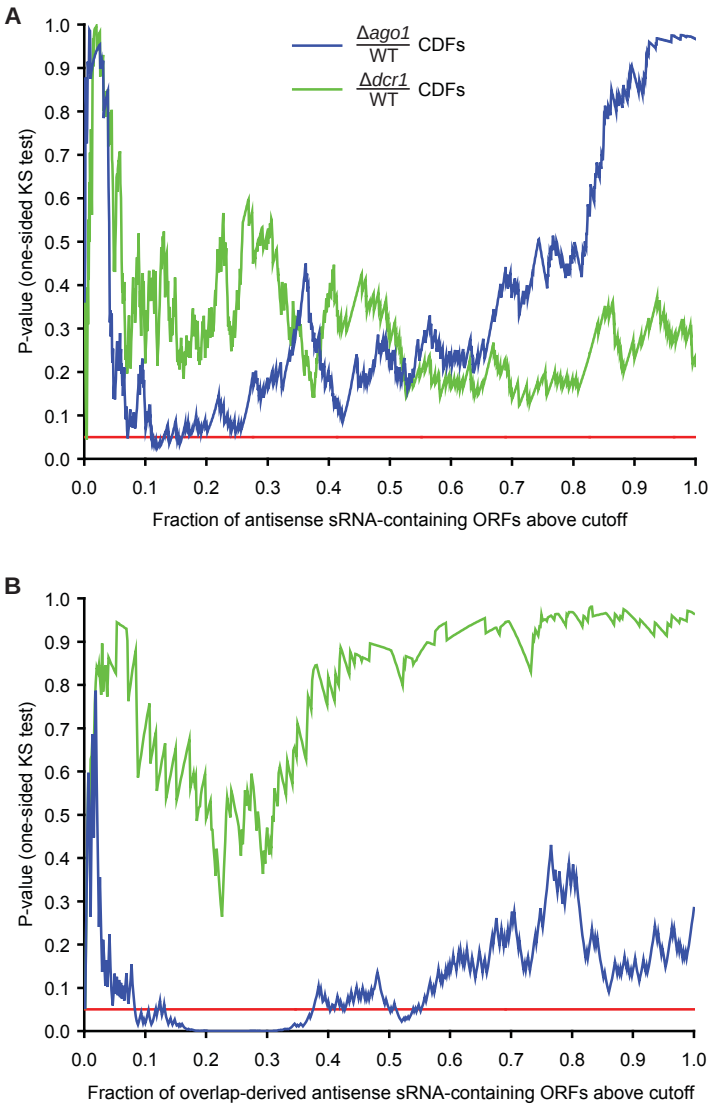

Figure S6. Impact of siRNAs on ORF-containing transcripts. **(A)** Statistical analysis of the impact of small RNAs (sRNAs) mapping antisense to annotated ORFs. ORFs were sorted descending by antisense sRNAs per kb and the significance of transcript down regulation for the ORFs with greater numbers of small RNAs was calculated for the full range of cutoff values. A one-sided KS test was used to compare the distribution of Δ*ago1*/WT (blue) or Δ*dcr1*/WT (green) transcript ratios for ORFs above and below each cutoff. Plotted are the resulting P-values as a function of the cutoff (expressed as the fraction of all antisense-sRNA-containing ORFs included above the cutoff). The red line indicates the $P = 0.05$ significance cutoff. **(B)** Statistical analysis of the impact of sRNAs generated by overlapping convergent gene pairs. ORFs were sorted descending by overlapping-transcript-derived antisense sRNAs/kb and analyzed as in (A).

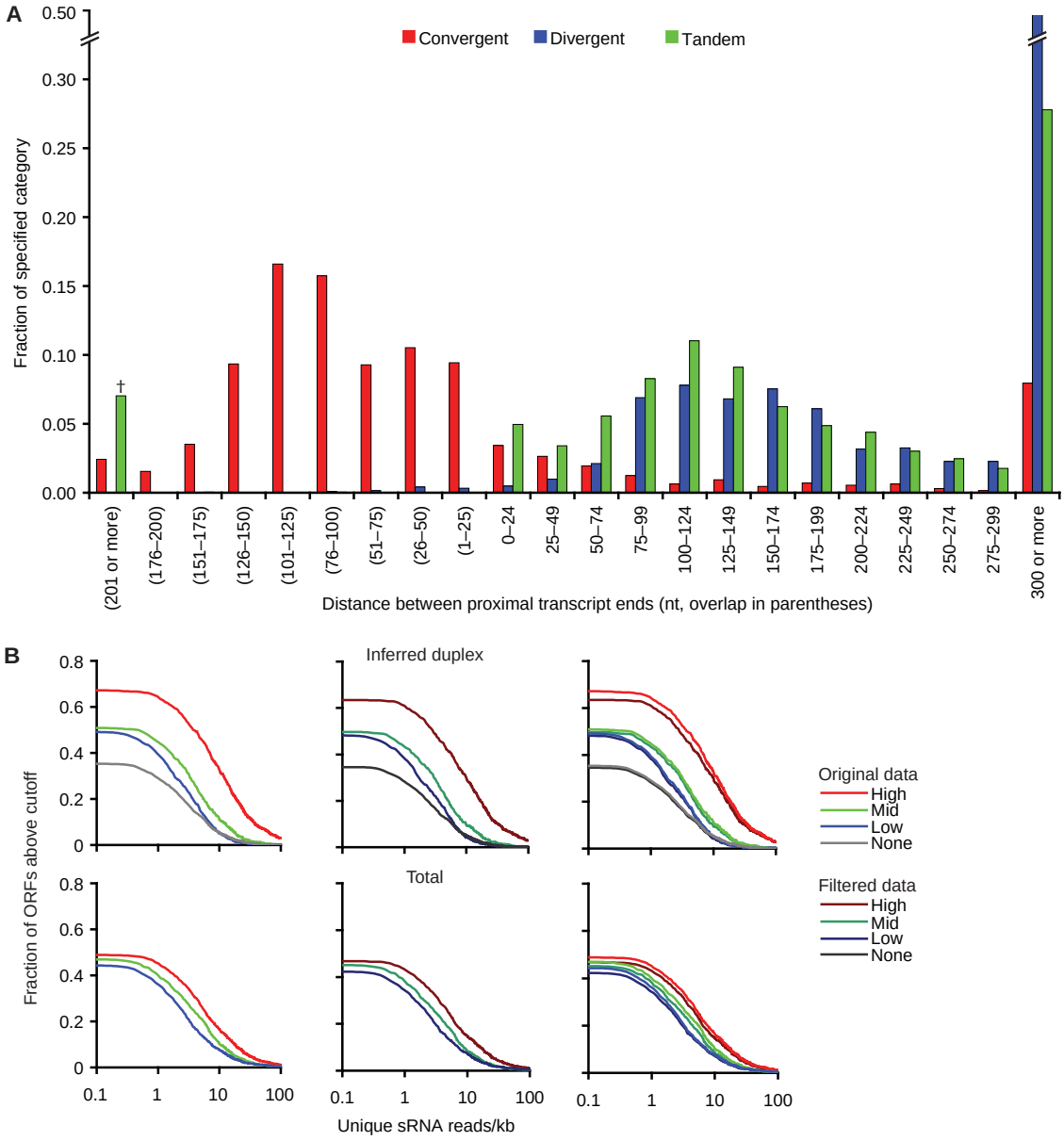

Figure S7. Gene-pair organization and overlap in *S. castellii*. **(A)** Distribution of gene-pair inter-transcript distances. Gene pairs were binned by the distance between 3′-ends (convergent), 5′-ends (divergent), or 3′-end of the upstream gene and 5′-end of the downstream gene (tandem). Plotted is the fraction of gene pairs of a given orientation category that fall within each bin. † For overlapping tandem gene pairs, transcript ends for both genes represent the 5′ and 3′ ends of the contiguous signal observed by mRNA-Seq. Therefore, tandem gene pairs are depicted as overlapping across their length. **(B)** Correlation between transcript abundance and small RNA density for annotated ORFs. ORFs were binned according to inferred duplex abundance (estimated as the abundance of the limiting strand; top) or total transcript abundance (sum of sense and antisense tags; bottom). Plotted is the fraction of ORFs within a given bin that have at least as many uniquely matching small RNA reads (on either strand) as the x-axis value. As expected if siRNAs in coding sequences derived from dsRNA precursors formed by sense-antisense transcript pairs, the abundance of ORF siRNAs correlated with the abundance of the inferred duplex. Filtered data excludes all convergent overlapping gene pairs that give rise to small RNAs in the overlap region .

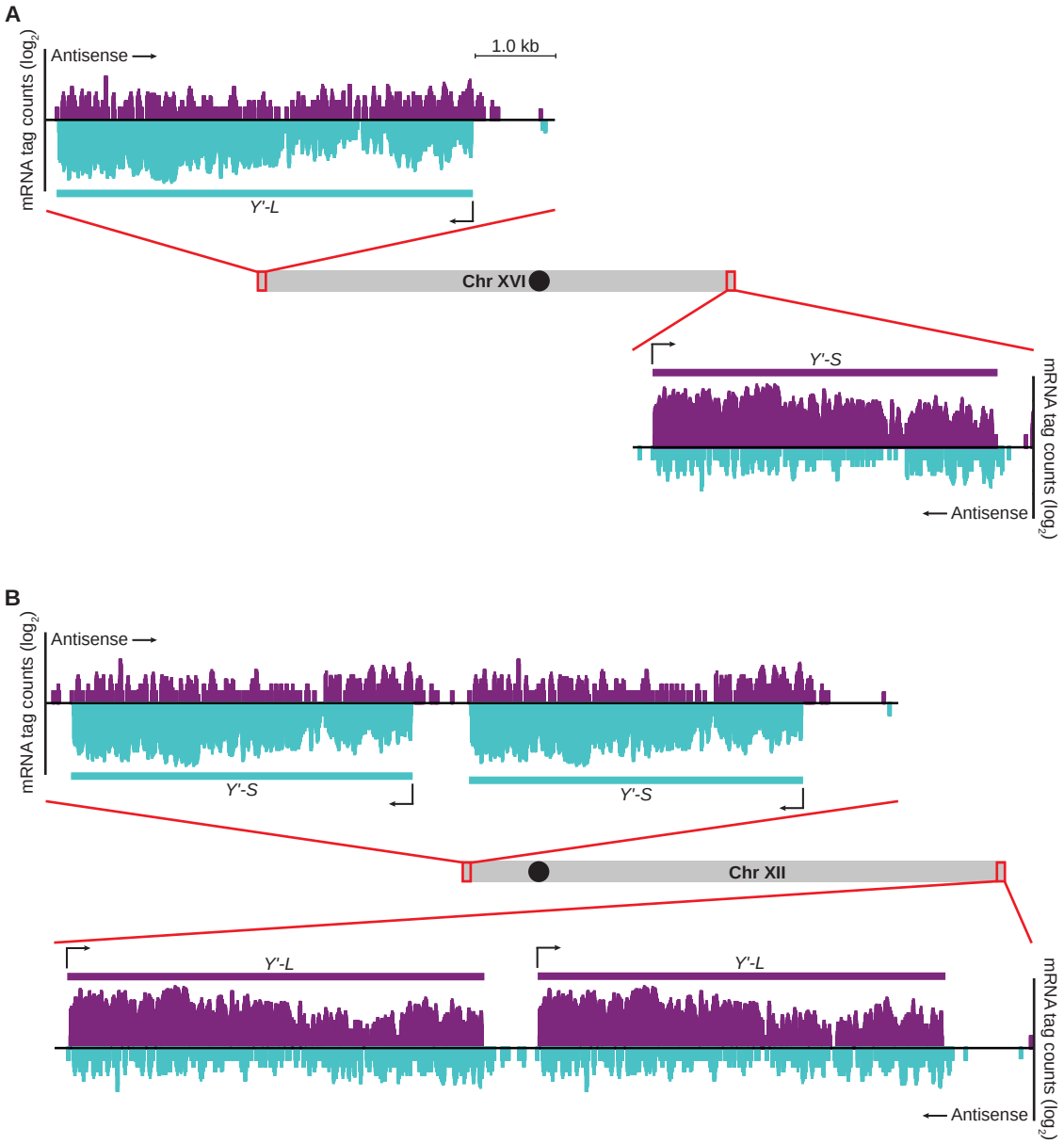

Figure S8. mRNA-Seq analysis of the *S. cerevisiae* Y′ elements. **(A)** Transcripts mapping to chromosome XVI subtelomeres. mRNA-Seq tags were mapped to the reference genome. Tags mapping to the subtelomeric regions of chromosome XVI are shown, with tags contributing to the counts along their entire length. Positions of the vertical axes correspond to the ends of the chromosome. *Y′-L* and *Y′-S* represent the inferred genes corresponding to the long and short isoforms of *S. cerevisiae* Y′ elements, respectively. In *S. cerevisiae*, the telomeres are transcriptionally silenced by Sir2-dependent heterochromatin but still give rise to low levels of cryptic transcripts that are rapidly degraded by the TRAMP and exosome complexes (*S28*). The previously characterized *S. cerevisiae* cryptic telomeric transcripts are ~6.5 kb in length, and begin near chromosome ends and run antisense through the entire Y′-element ORF. The antisense reads we detected across *S. cerevisiae* subtelomeric regions may represent these previously identified cryptic transcripts. **(B)** Transcripts mapping to chromosome XII subtelomeres. Plots are as in (A).

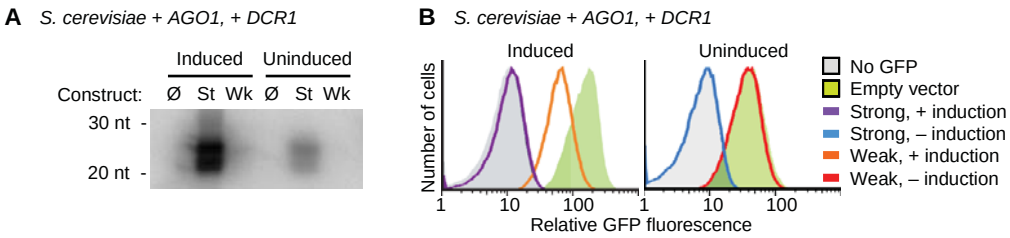

Figure S9. Reconstituting RNAi in *S. cerevisiae*. **(A)** Northern blot for siRNAs antisense to GFP in a *S. cerevisiae* strain expressing *S. castellii AGO1*, *DCR1*, and either no silencing construct (Ø), an integrated strong silencing construct (St), or an integrated weak silencing construct (Wk). Cells were induced in SC media with galactose and raffinose or uninduced in SC media with glucose. **(B)** FACS histograms of GFP fluorescence in *S. cerevisiae* expressing *S. castellii AGO1* and *DCR1* and the indicated silencing constructs. The same cultures were used here for sorting as for RNA collection in (A). In principle the siRNAs and silencing observed under uninduced conditions could be due to leaky expression from the *GAL1* promoter, but these effects are probably attributable to constitutive antisense transcription from a downstream promoter.

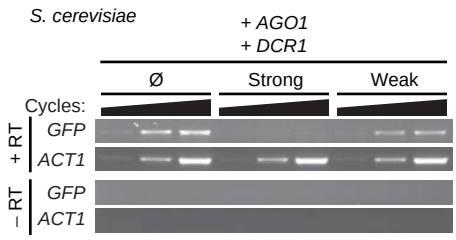

Figure S10. Analysis of *GFP* mRNA in reconstituted RNAi in *S. cerevisiae*. Aliquots from RT-PCR reactions were removed after increasing numbers of PCR cycles (*GFP*: 28, 32, 36; *ACT1*: 24, 28, 32) and visualized by ethidium bromide staining.

A

Plasmid	WT	Δ*ago1*	Δ*dcr1*
CEN	300	5	10
2μ	105	11	7
2μ Ago1	225	7	25
2μ Ago1, induced	169	96	4
2μ Dcr1	169	9	11
2μ Dcr1, induced	142	2	127

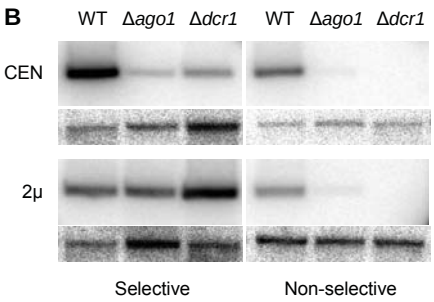

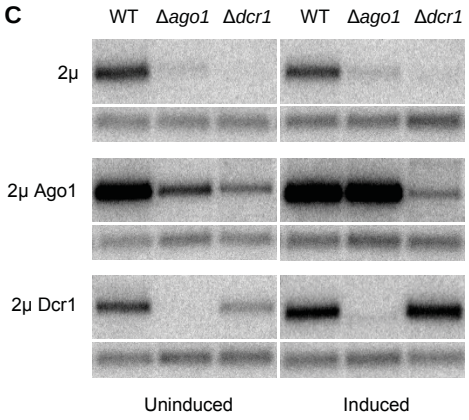

Figure S11. Plasmid instability in RNAi mutants. **(A)** Number of colonies obtained upon transformation of each strain with the plasmid indicated, sum of three independent transformations (table S6). The CEN plasmid was pRS316; 2μ was a 2-micron origin plasmid; 2μ Ago1 and 2μ Dcr1 were 2-micron plasmids expressing Ago1 or Dcr1, respectively, under the *S. cerevisiae* GAL1 promoter. **(B)** Southern blot for abundance of the indicated plasmid in each of the indicated strains. Plasmids (CEN, 2μ) were detected with a probe against the ampicillin-resistance gene; loading controls (thin panels) were probed for a genomic locus. DNA was isolated from cells grown in SC–ura (selective) or YPD (non-selective). **(C)** Southern blot probed as in (B) monitoring rescue of plasmid maintenance phenotype using DNA isolated from cells grown in YPD (uninduced) or YP-galactose (induced).

Δ*ago1* and Δ*dcr1* mutants yielded fewer colonies upon plasmid transformation than did wild-type *S. castellii* (fig. S11A, top two rows). This effect was observed for CEN plasmids (which contained an *S. cerevisiae* centromere sequence and an *S. cerevisiae* chromosomal origin of replication) as well as 2-micron plasmids (which contained the origin of the *S. cerevisiae* endogenous 2-micron circle but no centromere sequence). To distinguish whether this effect reflected a defect in plasmid transformation (plasmid entering the cell) or plasmid maintenance (propagation of the plasmid after entering the cell), we attempted to rescue the defect by transforming wild-type, Δ*ago1*, and Δ*dcr1* strains with plasmids expressing either Ago1 or Dcr1 from an inducible promoter. If the mutant strains were defective in transformation, then these Ago1 and Dcr1 expression plasmids would not enter the cell and thus could not rescue the mutant phenotype. Alternatively, if the mutant strains were defective in plasmid maintenance, then these plasmids would enter the cell, and expression of plasmid-borne Ago1 or Dcr1 in the cognate mutant could rescue maintenance of the expression plasmid itself. When the Δ*ago1* mutant was transformed with the Ago1-expression plasmid and the cells were plated on inducing media, wild-type numbers of colonies were obtained. The same was observed for the Δ*dcr1* mutant transformed with the Dcr1-expression plasmid. This rescue was not observed with the non-cognate plasmids or when expression was not induced (fig. S11A), thereby demonstrating the specificity of the rescue. These results show that RNAi is required for maintenance of *S. cerevisiae* plasmids in *S. castellii*.

We then used Southern blots to monitor plasmid levels. For the CEN plasmid, Δ*ago1* and Δ*dcr1* mutants carried, on average, fewer plasmids per cell relative to wild-type cells, even when grown in selective media (fig. S11B, top). For the 2-micron plasmid, Δ*ago1* and Δ*dcr1* mutants maintained the plasmid at wild-type abundance in selective media, although growth was considerably slower. When allowed to lose plasmid by growth in rich, non-selective media, the mutants lost more plasmid than the wild-type cells did (fig. S11B, bottom). Consistent with the rescue observed when counting colonies (fig. S11A), expressing the relevant protein from the plasmid being monitored rescued the plasmid-maintenance phenotype (fig. S11C). Partial rescue was observed without induction due to leaky expression, but full rescue required induction.

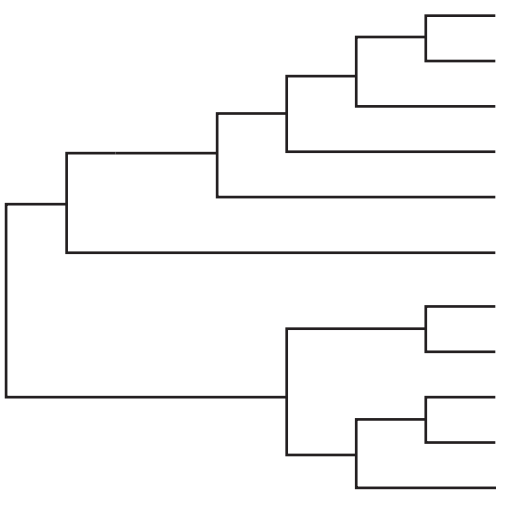

	copia family*	gypsy family: Ty3-like	gypsy family: Tca3-like
Saccharomyces cerevisiae	53	2	0
Saccharomyces bayanus	10	0	0
Candida glabrata	0	1	0
Saccharomyces castellii	8	10	8
Kluyveromyces polysporus	18	8	16
Zygosaccharomyces rouxii	0	2	0
Kluyveromyces lactis	2	0	0
Ashbya gossypii	0	1	0
Kluyveromyces waltii	25	3	0
Kluyveromyces thermotolerans	2	0	0
Saccharomyces kluyveri	9	0	0

* Ty1, Ty2, Ty4, Ty5

Figure S12. Approximate copy numbers of retroelements in budding yeast species. Copy numbers were estimated by TBLASTN searches using the Gag-Pol polyprotein as a search query. Intact genes and pseudogenes were counted, but not solo LTRs. *S. castellii* and *K. polysporus* have many more Ty3/gypsy elements (18 and 24 elements, respectively) than those budding yeast species that have lost the RNAi pathway (0–3 elements). Most notably, a subfamily of gypsy elements more similar to *C. albicans* Tca3 (*S29*) than to *S. cerevisiae* Ty3 is found exclusively in species that have retained the RNAi pathway: *S. castellii* and *K. polysporus*, as well as several *Candida* species. The two gypsy subfamilies have been proposed to have different mechanisms for priming minus-strand RNA synthesis (*30*). As in *C. albicans*, many of the members of the gypsy families in *S. castellii* and *K. polysporus* appear to be structurally rearranged. It is possible that selection has favored the retention of these structures as templates for defensive siRNA production.

Table S1. Analysis of small-RNA libraries. Read counts were normalized to the number of genomic matches and separated into different cateories based on genome annotations and alignments. Numbers in parenthesis are percent of reads compared to number of genome matching reads of either all sequence reads or only reads of 21–23-mers.

	S. castellii				*K. polysporus*		*C. albicans*		*S. cerevisiae*	
	wild-type		*Δago1*	*Δdcr1*						
Annotation	all reads	21–23-mers	all reads	all reads	all reads	21–23-mers	all reads	21–23-mers	all reads	21–23-mers
Ty retrotransposons										
Palindromic	27984.0 (12.1)	24419.2 (22.5)	81.0 (0.1)	11.3 (<0.1)	5891.5 (0.7)	5020.2 (1.6)	0.0 (0.0)	0.0 (0.0)	0.0 (0.0)	0.0 (0.0)
Non-palindromic	18949.8 (8.2)	16223.0 (14.9)	271.1 (0.3)	9662.6 (0.8)	98666.5 (11.2)	79859.1 (25.5)	881.5 (0.1)	677.0 (0.3)	52.8 (<0.1)	3.9 (<0.1)
Y′ elements	4942.9 (2.1)	4172.5 (3.8)	9.0 (0.0)	50.0 (<0.1)	67354.8 (7.6)	56305.0 (18.0)	–	–	10.8 (<0.1)	1.0 (<0.1)
Zorro3	–	–	–	–	–	–	4809.5 (0.4)	3416.0 (1.6)	–	–
CTA2 family	–	–	–	–	–	–	8991.9 (0.8)	6848.9 (3.1)	–	–
LPF family	–	–	–	–	–	–	2198.5 (0.2)	1604.0 (0.7)	–	–
Other transposon homology *	–	–	–	–	–	–	1719.1 (0.1)	1226.0 (0.6)	–	–
Other palindromes	18322.2 (7.9)	16356.7 (15.0)	51.0 (0.1)	23.5 (<0.1)	20503.5 (2.3)	17039.3 (5.4)	–	–	–	–
ORF clusters	1860.2 (0.8)	1583.9 (1.5)	8.7 (<0.1)	45.3 (<0.1)	11114.0 (1.3)	9170.6 (2.9)	2972.6 (0.25)	2080.1 (1.0)	–	–
Other siRNA clusters	15191.2 (6.5)	13267.8 (12.2)	87.0 (<0.1)	6977.3 (0.6)	39390.4 (4.5)	31612.7 (10.1)	8487.0 (0.7)	5367.5 (2.5)	–	–
ORFs	2829.4 (1.2)	1971.5 (1.8)	123.7 (0.1)	23616.4 (1.9)	9094.7 (1.0)	5568.7 (1.8)	19253.8 (1.6)	8131.6 (3.7)	3783.1 (1.0)	700.2 (1.0)
Pseudogenes	n.d.	n.d.	n.d.	n.d.	73.4 (<0.1)	48.0 (<0.1)	n.d.	n.d.	5.2 (<0.1)	2.0 (<0.1)
Centromeres	n.d.	n.d.	n.d.	n.d.	n.d.	n.d.	15.0 (<0.1)	0.0 (0.0)	0.0 (0.0)	0.0 (0.0)
Telomeres	n.d.	n.d.	n.d.	n.d.	2284.2 (0.3)	1817.5 (0.6)	n.d.	n.d.	0.2 (<0.1)	0.0 (0.0)
Non-protein coding RNAs										
rRNA	103905.9 (44.7)	19039.8 (17.5)	74687.1 (76.2)	746407.5 (62.7)	525501.2 (59.6)	80098.5 (25.6)	990056.6 (83.2)	148932.0 (68.0)	310004.5 (84.9)	63278.7 (87.4)
tRNA	3550.4 (1.5)	565.2 (0.5)	2635.4 (2.7)	98132.5 (8.2)	63408.8 (7.2)	8267.0 (2.6)	39074.3 (3.3)	6225.0 (2.8)	38398.3 (10.5)	6140.0 (8.5)
Other ncRNA	n.d.	n.d.	n.d.	n.d.	n.d.	n.d.	30297.8 (2.5)	6309.0 (2.9)	2339.4 (0.6)	431.0 (0.6)
Other	34680.1 (14.9)	11169.5 (10.3)	19997.0 (20.4)	305659.6 (25.7)	30565.8 (3.5)	13249.4 (4.2)	80747.5 (6.8)	28135.0 (12.8)	10691.7 (2.9)	1869.2 (2.6)
Total genome-matching reads	232226.0 (100)	108769.0 (100)	97951.0 (100)	1190586.0 (100)	881041.0 (100)	312884.0 (100)	1189505.0 (100)	218952.0 (100)	365286.0 (100)	72426.0 (100)
Total reads	510234		528020	4265687	1777358		3334405		1227275	

* Hypothetical protein CaO19.7545, potential SWIM zinc finger protein very similar to CaP19.4241, C terminus is same as Rel-associated hypothetical protein, MULE transposase domain; Hypothetical protein CaO19.6608, weak similarity to C. albicans Cirt2 transposase

n.d. - not determined

– - not applicable

Table S2. Analysis of small-RNA libraries from input and $Flag_3$-Ago1 IP datasets. Read counts were normalized to the number of genomic matches and separated into different cateories based on genome annotations and alignments. Numbers in parentheses are percent of reads compared to number of genome matching reads of either all sequence reads or only reads of 22–23-mers.

	Input				$Flag_3$-Ago1 IP			
	all reads		22–23-mers		all reads		22–23-mers	
Ty retrotransposons								
Non-palindromic Ty	23892.9	(1.7)	15310.0	(3.8)	53793.7	(4.5)	40818.3	(5.2)
Palindromic Ty	110728.9	(7.7)	75986.0	(19.0)	281476.6	(23.7)	213975.9	(27.2)
Y′ elements	14058.9	(1.0)	9037.7	(2.3)	29293.5	(2.5)	21335.9	(2.7)
Other palindromes	70149.7	(4.9)	51205.4	(12.8)	164269.9	(13.9)	128153.5	(16.3)
ORF clusters								
Sense ORF clusters	7172.8	(0.5)	3530.2	(0.9)	13191.2	(1.1)	10197.4	(1.3)
Antisense ORF clusters	17705.9	(1.2)	11774.5	(2.9)	38322.0	(3.2)	29345.9	(3.7)
Overlapping mRNAs	4958.4	(0.3)	2106.5	(0.5)	9251.8	(0.8)	7028.0	(0.9)
Other siRNA clusters	135377.1	(9.4)	90559.8	(22.6)	368810.2	(31.1)	269707.6	(34.3)
Open reading frames								
Sense ORFs	244127.2	(16.9)	29220.9	(7.3)	49693.8	(4.2)	13907.4	(1.8)
Antisense ORFs	20280.8	(1.4)	5033.7	(1.3)	18576.6	(1.6)	9380.3	(1.2)
tRNA	66699.1	(4.6)	5629.7	(1.4)	3573.7	(0.3)	244.4	(<0.1)
rRNA	479478.7	(33.3)	68866.7	(17.2)	101753.5	(8.6)	20168.2	(2.6)
Other	245917.5	(17.1)	32093.0	(8.0)	53441.5	(4.5)	22434.4	(2.9)
Total genome-matching reads	1440548	(100)	400354	(100)	1185448	(100)	786697	(100)
Total reads	4310251				4102562			

Table S3. siRNA-producing loci and their transcripts. Start and end represent the inferred 5′ and 3′ ends of the transcript, respectively. Coverage is the percentage of nucleotides in the transcript (excluding nucleotides added during fine mapping) that are represented by mRNA-Seq tags.

	Inferred Precursor Transcript				
Cluster coordinates	Strand	Name	Start	End	Coverage (%)
sc1:429–661	+		429	661	82.4
	–		661	429	85.8
sc2:68–238	+		58	238	25.4
	–	*NCS33*	468	58	96.8
sc196:342–609	+		342	609	0.0
	–		649	122	95.3
sc276:74–1288	+		34	1303	33.8
	–	*NCS42*	1288	24	83.2
sc335:46–172	+		46	172	48.8
	–		172	46	46.5
sc335:463–721	+		463	721	9.7
	–	*NCS84*	873	363	98.2
sc345:1–432	+		1	441	78.5
	–		432	1	48.4
sc360:1541–1647	+	*NCS85*	1351	1672	100.0
	–		1647	1541	0.0
sc365:495–600	+		44	620	98.9
	–		870	475	86.6
sc375:37–696	+		37	766	94.1
	–		696	37	26.5
sc377:1723–2191	+		1723	2191	16.0
	–		2301	1343	95.9
sc382:317–1193	+		317	1193	57.8
	–		1193	244	78.9
sc388:360–581	+		360	581	22.5
	–		601	250	86.9
sc388:833–1511	+		833	1511	14.7
	–		1511	833	7.4
sc391:1088–1185	+		1078	1235	90.5
	–		1235	1068	81.5
sc391:1935–2433	+		1935	2433	51.5
	–		2453	1895	72.8
sc409:577–712	+		557	722	84.3
	–		712	577	18.4
sc412:1789–1960	+		1643	2138	100.0
	–		1960	1789	0.0
sc413:1937–2027	+		1157	2037	99.9
	–		2717	1899	100.0
sc419:1286–1358	+	*NCS72*	1262	1518	100.0
	–		1398	1286	44.2
sc425:395–1034	+		395	1034	15.9
	–	*NCS21*	1184	225	93.2
sc425:1295–2077	+		1295	2077	10.5
	–	*NCS19*	2127	1215	86.6
sc435:32–1092	+		32	1552	90.9
	–		1092	32	73.6
sc435:1977–2192	+		1917	2312	83.6
	–		2192	1977	23.1
sc435:2434–2662	+		2434	2772	83.2
	–		2662	2434	21.8
sc436:1030–1361	+		990	1881	100.0
	–		1361	1030	0.0
sc437:3822–4066	+		3815	4072	98.8
	–	*NCS77*	4396	3822	96.9
sc438:1–1441	+		1	1441	76.3
	–		1454	1	73.5
sc441:660–812	+		660	812	0.0
	–	*NCS39*	895	450	96.4
sc451:79–2774	+		66	3234	84.7
	–		2774	79	77.1
sc455:5844–5967	+		5844	5967	0.0
	–	*NCS61*	6309	5442	99.0
sc462:65–1252	+		65	1252	85.9
	–		1252	65	76.4
sc462:1642–2097	+		1642	2097	0.0
	–		2098	1362	91.3
sc471:5550–5778	+		5550	5778	28.4
	–	*NCS76*	5870	5190	99.9
sc471:6204–6659	+	*NCS53*	6204	6734	87.1
	–		6659	5114	86.1
sc473:1270–2094	+		1055	2134	100.0
	–		2094	1270	11.6
sc473:2266–2389	+		666	2779	99.7
	–		2389	2266	0.0
sc474:2097–2411	+		2010	2960	100.0
	–		2411	2097	31.7
sc474:5702–6100	+		5702	6140	45.8
	–		6100	5177	96.8
sc476:6759–7299	+		6679	7389	86.2
	–		7299	6759	16.3
sc476:7961–8182	+		7941	8292	83.2
	–		8182	7961	22.5
sc485:8485–9090	+		8475	9180	86.3
	–		9090	8485	23.9
sc490:8033–8385	+		8033	8385	7.1
	–		8410	7163	100.0
sc490:9427–9629	+	*NCS74*	9127	9957	100.0
	–		9629	9427	12.3
sc493:8255–8723	+		8255	8743	32.7
	–		8893	7675	95.7
sc497:9649–10263	+		9649	10263	68.5
	–	*NCS10*	10263	9189	98.3
sc502:4–583	+		1	583	21.4
	–		623	1	100.0
sc502:753–1055	+		753	1055	8.3
	–		1075	625	100.0
sc506:13783–13836	+		13783	14092	94.8
	–		13837	13783	100.0
sc508:7282–7527	+		7276	7533	100.0
	–	*NCS79*	7760	7282	97.9
sc509:188–473	+		158	503	70.2
	–		533	188	54.9
sc509:9632–9853	+		9632	9963	77.4
	–		9853	9632	11.3
sc509:10321–10542	+		10301	10602	87.4
	–		10542	10321	22.5
sc511:11–213	+		11	213	0.0
	–		213	1	46.5
sc517:Feb–16	+		1	3786	73.6
	–	*NCS35*	2516	1	71.7
sc517:4869–5249	+		4779	5279	49.7
	–		5249	4859	72.4
sc517:5592–6682	+		5572	7096	97.8
	–		6682	5592	54.5
sc517:6922–7017	+		6144	7040	99.8
	–		7017	6922	26.0
sc517:7607–7752	+		7607	7752	0.0
	–		7752	7327	83.8
sc519:294–618	+		294	618	21.8
	–		1118	290	98.2
sc522:1143–1744	+		1143	1744	8.3
	–		1744	1083	75.4
sc523:Oct–05	+		1	2705	76.3
	–		2718	1	82.2
sc523:2962–3417	+		2962	3417	0.0
	–		3418	2742	92.2
sc523:5224–5445	+		5224	5445	11.3
	–		5495	5151	95.0
sc525:4218–4572	+		4218	4572	7.6
	–		4945	3958	100.0
sc527:4128–4728	+		4128	4728	50.7
	–	*NCS17*	4768	4028	99.2
sc528:14255–14336	+		13315	14342	100.0
	–		14676	14245	97.7
sc534:69–1432	+		68	1432	87.5
	–		1432	1	76.7
sc534:1822–2277	+		1822	2277	0.0
	–		2278	1592	89.5
sc534:8952–9353	+		8912	9353	17.8
	–	*NCS67*	9503	8922	80.4
sc534:9993–10089	+		9993	10089	0.0
	–		10089	9863	84.6
sc534:10195–10626	+		10195	10626	0.0
	–		10626	10115	71.1
sc535:1–1222	+		1	1222	71.5
	–		1235	1	76.3
sc535:1479–1920	+		1479	1920	0.0
	–		1940	1249	86.7
sc537:2001–2167	+		1906	3987	99.9
	–		2167	2001	0.0
sc539:159–405	+	*NCS80*	1	405	97.5
	–		411	153	100.0
sc539:1276–1703	+		1276	1703	0.0
	–		1825	1255	96.8
sc542:764–929	+		764	929	0.0
	–		929	764	51.2
sc542:1579–1684	+		1579	1684	0.0
	–		1684	1579	34.9
sc542:6091–6205	+		5091	6221	100.0
	–		6205	6081	63.2
sc542:14947–15985	+		14947	16130	91.3
	–		15985	14947	24.5
sc542:16197–18913	+		16197	19025	63.4
	–		18913	16156	89.2
sc547:13848–14000	+		13848	14000	38.6
	–		14000	13828	50.3
sc549:16769–17410	+		16569	17440	80.3
	–		18397	16769	83.2
sc553:36–669	+		36	669	53.0
	–		1231	36	79.8
sc553:926–1381	+		926	1381	0.0
	–		1382	696	92.9
sc553:3188–3409	+		3188	3409	22.5
	–		3429	3078	86.9
sc558:9896–10121	+		9896	10191	89.2
	–		10121	9896	11.1
sc558:11930–12385	+		11920	12535	90.1
	–		12385	11930	0.0
sc558:12604–12822	+		12604	12932	78.1
	–		12822	12604	11.4
sc559:825–1331	+		813	1481	100.0
	–		1331	815	16.4
sc559:8888–9015	+		8878	9055	55.6
	–		9255	8888	73.1
sc561:20642–20871	+		20602	20947	93.4
	–		20871	20642	10.9
sc562:19159–19222	+		18169	19262	99.8
	–		19562	19149	95.4
sc565:20405–20997	+		20405	21027	36.9
	–	*NCS51*	20997	20365	77.4
sc565:21201–21383	+		21181	21383	82.8
	–		21413	21191	87.4

Continued on next page

Table S3, continued

Cluster coordinates	Inferred Precursor Transcript				
	Strand	Name	Start	End	Coverage (%)
sc565:21580–21803	+		21520	21891	66.1
	–		21803	21510	85.0
sc567:20621–20981	+		20141	20981	80.5
	–		21231	20621	97.2
sc568:18314–18566	+		18283	18616	95.5
	–		18566	18184	65.0
sc575:5776–5935	+		4986	5947	100.0
	–		6075	5776	88.0
sc578:13092–13331	+		13092	13331	45.8
	–		13363	12852	95.7
sc580:2233–4179	+	*NCS31*	2233	4179	98.9
	–		4179	2213	26.0
sc582:23773–24238	+	*NCS43*	23733	24309	78.3
	–		24638	23662	99.5
sc582:24415–24595	+		24365	24645	76.9
	–		24638	23662	99.5
sc587:198–326	+		194	326	96.9
	–	*NCS27*	506	198	90.3
sc587:663–788	+		663	788	84.1
	–	*NCS28*	833	543	98.6
sc588:7386–7753	+		6836	7843	99.6
	–		8453	7306	94.2
sc588:30087–30218	+		30087	30218	0.0
	–		30348	29567	100.0
sc589:3374–3461	+		2794	3463	100.0
	–		5031	3354	100.0
sc589:20446–20656	+		20446	20656	0.0
	–		20826	20336	92.3
sc596:1304–1461	+		1304	1461	15.8
	–		1501	1064	100.0
sc600:9619–10607	+		9610	10607	1.6
	–	*NCS13*	11697	9287	99.9
sc600:10849–11141	+		10849	11141	0.0
	–	*NCS16*	11695	9779	100.0
sc604:4257–4935	+		4246	6113	99.0
	–		4935	4237	51.9
sc608:25105–25468	+		25095	25468	81.8
	–	*NCS81*	25650	25105	97.3
sc610:2400–2460	+		1999	2483	100.0
	–		2470	2400	62.3
sc610:21566–21806	+		21566	21846	17.8
	–		22616	21512	100.0
sc610:22108–22644	+		22068	22664	44.7
	–		22654	21512	99.0
sc618:9475–9557	+		7925	9574	100.0
	–		10191	9445	98.8
sc621:39720–39823	+		39720	39823	0.0
	–		39912	39090	99.8
sc621:40611–40703	+		40611	40703	0.0
	–		40799	39931	98.6
sc622:33321–33622	+		33201	33622	67.5
	–	*NCS69*	33882	33181	94.2
sc622:34331–34482	+	*NCS65*	34041	34703	97.7
	–		34482	34311	29.1
sc622:34908–35226	+	*NCS59*	34388	35226	95.5
	–		35246	34908	36.9
sc622:38796–39212	+		38796	39332	75.6
	–		39212	38796	24.0
sc622:39454–39682	+		39454	39742	80.3
	–		39682	39454	21.8
sc622:39899–40113	+		39889	40223	84.2
	–		40113	39899	23.3
sc623:4134–4482	+		4134	4482	7.2
	–		4543	3900	98.0
sc623:4774–5347	+		4774	6473	96.7
	–		5347	4764	35.9
sc623:33964–34329	+		32584	34329	99.4
	–		34334	33964	82.8
sc625:38090–38215	+		37338	38277	100.0
	–		38275	38090	55.4
sc626:1404–1897	+		1404	1907	28.8
	–		1897	1384	59.1
sc626:4673–7708	+		4623	7859	81.6
	–		7718	4653	26.3
sc626:9067–9601	+	*NCS58*	8967	9611	66.4
	–	*NCS57*	9601	8997	83.0
sc626:10146–10513	+		10146	10513	0.0
	–		10513	10146	0.0
sc626:14217–14526	+		14217	14526	27.4
	–		14526	14077	90.9
sc626:34543–34761	+		34523	34771	85.1
	–		34761	34543	22.8
sc630:49045–49132	+		48985	49144	94.9
	–		49132	49045	28.4
sc634:22393–22468	+		21616	22514	100.0
	–		23734	22391	99.3
sc635:14611–14845	+		14605	14858	100.0
	–		17485	14611	99.7
sc635:22395–24397	+		22395	24417	26.1
	–		24460	22275	92.9
sc639:6048–6314	+		5998	6604	100.0
	–		6314	6048	18.7
sc639:6526–6571	+		5996	6611	100.0
	–		6571	6516	44.6
sc639:11902–12807	+		11902	12847	74.2
	–		12807	11902	5.5
sc639:14024–14099	+		13733	14109	90.4
	–		14284	14001	100.0
sc640:9977–10500	+		9977	10500	0.0
	–		10665	9797	99.7
sc640:41728–41853	+		41238	41863	100.0
	–		41993	41728	94.7
sc641:11318–11523	+		10228	11523	88.7
	–		12033	11278	99.9
sc648:17560–17977	+		17560	17977	6.0
	–	*NCS49*	18172	16246	100.0
sc649:36–1264	+		36	1264	60.6
	–		1294	36	98.8
sc651:4–656	+	*NCS9*	1	1886	99.9
	–		656	1	4.9
sc651:1114–1851	+	*NCS8*	1	1891	99.9
	–	*NCS11*	1851	1114	55.4
sc651:3275–3339	+		2987	3355	100.0
	–		3399	3275	69.6
sc651:20127–20473	+		19223	20503	99.8
	–		20473	20127	0.0
sc653:7042–7296	+		6422	7579	94.6
	–		7296	7032	46.8
sc654:28406–28550	+		28386	28550	55.2
	–		29391	28226	99.8
sc654:55126–55305	+		54366	55305	96.2
	–		56633	55126	99.5
sc658:1329–1442	+		979	1493	96.9
	–		2808	1289	100.0
sc660:25974–26295	+		25574	26295	99.0
	–		26621	25964	99.2
sc660:34132–34683	+		34012	34868	99.8
	–		34784	34102	73.2
sc666:20702–20809	+		20202	20809	100.0
	–		20931	20702	100.0
sc666:32177–33508	+	*NCS23*	32167	33588	72.7
	–	*NCS24*	33508	32177	38.8
sc668:757–936	+		757	1000	82.1
	–		936	757	66.7
sc668:8927–8993	+		8587	9023	97.5
	–		11628	8907	99.9
sc668:14781–14990	+		14781	15020	57.1
	–		15110	14667	98.9
sc668:15296–15545	+		15286	15545	22.7
	–		15668	15186	99.6
sc673:19040–19451	+		19040	19451	45.6
	–		19451	18869	96.4
sc676:55494–55600	+		55454	55630	59.9
	–		55600	55494	23.4
sc676:55766–55886	+		55746	55886	35.5
	–		55886	55766	0.0
sc676:64085–64882	+		63565	64882	60.5
	–	*NCS40*	65004	64085	77.1
sc682:2205–2503	+		1985	3114	94.9
	–		2503	2205	0.0
sc682:24064–24178	+		23038	24198	98.8
	–		25038	24052	100.0
sc682:71530–71636	+		71040	71646	100.0
	–		71656	71530	55.1
sc683:12949–13534	+		12909	13584	58.1
	–	*NCS41*	13545	12949	86.4
sc686:19278–19559	+		19218	19589	78.0
	–		19639	19278	61.6
sc686:23938–26333	+		23918	26363	59.3
	–	*NCS26*	26334	23938	65.2
sc687:39–239	+		39	239	0.0
	–		239	29	53.1
sc687:770–991	+		770	991	22.5
	–		1011	760	84.1
sc687:1246–1450	+		1246	1460	23.3
	–		1490	1186	86.6
sc687:7487–8354	+		7417	8354	19.6
	–	*NCS60*	8704	7356	92.4
sc687:9826–10082	+		9826	10082	10.9
	–		10082	9826	0.0
sc687:59448–59803	+		59428	59833	97.3
	–		60023	59418	99.0
sc687:80365–80851	+		80365	80851	10.3
	–		81831	80293	96.4
sc687:81469–81624	+		81469	81624	0.0
	–		81825	80487	100.0
sc687:83334–83489	+	*NCS70*	83014	83622	98.3
	–		83489	83334	0.0
sc689:59311–59545	+		59311	59545	0.0
	–		59922	59006	100.0
sc695:29108–29282	+		27808	29312	94.0
	–	*NCS47*	29292	29108	96.0
sc696:31624–32479	+		31624	32479	15.8
	–		32479	31564	44.3
sc696:54775–54953	+		54775	54953	14.0
	–		55433	54695	100.0
sc696:58976–59060	+		58346	59079	99.9
	–		60430	58956	99.7
sc696:100414–100848	+	*NCS36*	99638	101123	99.9
	–		100848	100414	19.8
sc696:101156–101809	+	*NCS2*	101136	101809	94.8
	–	*NCS1*	101912	101156	98.4

Continued on next page

Table S3, continued

Cluster coordinates	Inferred Precursor Transcript				
	Strand	Name	Start	End	Coverage (%)
sc697:26569–26676	+		25879	26686	99.7
	–		27214	26569	98.4
sc701:29781–29871	+		29356	29891	100.0
	–		29941	29781	53.4
sc701:57551–57929	+	*NCS64*	57431	57929	87.5
	–		57939	57551	40.4
sc701:83724–83892	+		82724	83892	93.7
	–		84282	83714	100.0
sc709:24929–25083	+		24738	25083	89.9
	–		25357	24920	100.0
sc709:28052–28465	+		27952	28485	74.0
	–		29028	28002	96.4
sc709:43781–43874	+		43171	43874	92.0
	–		44304	43751	100.0
sc709:69749–70066	+		69159	70396	100.0
	–		70066	69739	4.7
sc709:86133–86705	+		86003	86766	70.2
	–		86825	85513	91.6
sc710:8141–8912	+		7781	9082	93.1
	–		8912	8121	82.1
sc710:12032–12080	+		12002	12080	82.3
	–		12080	12032	0.0
sc710:12346–12436	+		12236	12436	80.1
	–		12436	12346	0.0
sc710:12948–13955	+	*NCS5*	12948	14355	99.4
	–		13955	12948	25.0
sc710:36397–37654	+		36327	37704	86.4
	–		37654	36397	7.9
sc710:37835–38239	+		37813	38259	96.2
	–		38249	37835	21.9
sc710:38873–40259	+		38873	40279	11.1
	–	*NCS34*	40259	38864	98.7
sc710:126921–127123	+		126651	127123	87.9
	–		128033	126921	97.6
sc712:108122–108755	+		108122	108755	27.9
	–		108835	107733	96.0
sc712:125879–125996	+	*NCS55*	125569	126026	100.0
	–		126958	125879	99.0
sc714:111363–111513	+		111353	111513	15.5
	–	*NCS45*	111523	111353	100.0
sc714:112909–112975	+		112049	112988	99.9
	–		113325	112909	90.2
sc716:28464–28791	+	*NCS14*	28444	29886	96.8
	–		28791	28444	14.4
sc716:29088–29402	+	*NCS15*	28657	29886	99.8
	–		29402	29088	0.0
sc716:159394–159521	+		158574	159531	99.4
	–		160538	159389	100.0
sc719:52927–53456	+		52927	53456	0.0
	–		53603	52707	91.9
sc719:80550–80667	+		78360	80677	100.0
	–		81447	80550	95.5
sc719:80983–81279	+		80983	81309	15.3
	–		81449	80582	98.8
sc719:145408–145856	+		145408	145907	67.7
	–		145866	145408	18.3
sc719:188938–189063	+		187376	189093	98.8
	–		190169	188926	99.5
sc720:16982–17198	+		16912	17198	84.7
	–		17848	16962	100.0
sc720:17512–17778	+		17512	17788	70.8
	–		17848	16972	100.0
sc720:86102–86250	+		85842	86250	100.0
	–		87980	86102	99.4
sc721:29938–30311	+		29938	30311	0.0
	–		30351	29888	59.5
sc721:30729–30988	+		30699	30988	64.5
	–		31018	30719	70.0
sc721:31159–32062	+		31149	32122	89.8
	–	*NCS44*	32082	31159	74.8
sc721:42216–43245	+		42201	43340	100.0
	–		43255	42216	25.7
sc721:83771–84102	+		83771	85392	99.3
	–		84102	83771	30.1
sc721:87525–88833	+		87525	88833	10.5
	–		89781	87375	98.0
sc721:104062–104151	+		102375	104181	99.9
	–		105461	104052	99.4
sc721:140124–140427	+		139464	140450	100.0
	–		140577	140124	98.2
sc721:145814–145981	+		145784	145981	69.1
	–		147571	145814	97.1
sc721:191325–191431	+		191135	193881	100.0
	–		191431	191325	0.0
sc721:193779–194025	+		192279	194025	99.4
	–		194030	193773	100.0
sc721:210477–210897	+		210430	211350	100.0
	–		210897	210477	5.9
sc721:277776–277936	+		277616	278030	100.0
	–		277986	277776	39.8
sc1001:29178–29235	+		28748	29235	97.5
	–		29765	29148	100.0
sc1003:4321–4694	+		4260	4704	96.4
	–		5464	4321	97.6
sc1004:15739–15963	+		14289	15963	98.0
	–		16687	15739	91.4
sc1005:16254–16496	+		15514	16536	99.5
	–		16496	16214	74.9
sc1007:9377–9627	+		9370	12730	100.0
	–		9627	9377	0.0
sc1007:20870–21184	+		20830	21254	85.9
	–		21184	20870	46.0
sc1007:47015–47100	+		43965	47137	100.0
	–		47963	47015	99.0
sc1007:82752–82976	+		82752	82976	23.1
	–		82976	82752	0.0
sc1009:8540–8765	+		8235	8765	89.2
	–		9265	8531	100.0
sc1009:34804–35229	+		34804	35499	67.5
	–		35229	34784	10.8
sc1009:48729–49028	+		48729	49058	42.4
	–		49078	48634	99.8
sc1009:49220–49458	+		49210	49471	98.8
	–	*NCS68*	50968	49220	99.5
sc1013:2878–3451	+		2878	3451	4.4
	–		3467	1323	99.4
sc1014:32074–32342	+		32004	32422	74.7
	–		32342	32064	41.9
sc1014:33081–33362	+		32991	33373	100.0
	–		33372	33051	39.1
sc1014:55954–56360	+	*NCS30*	55804	56430	100.0
	–		56360	55954	0.0
sc1014:57720–60475	+		57700	60475	38.1
	–	*NCS25*	60505	57720	60.7
sc1014:62249–63722	+		62249	63722	10.2
	–		63722	62239	11.0
sc1014:69378–71630	+	*NCS4*	69378	71694	76.4
	–	*NCS3*	71630	69318	99.0
sc1014:84431–84529	+		83571	84531	100.0
	–		84875	84412	100.0
sc1014:118810–119191	+		118810	119561	90.2
	–		119211	118800	36.4
sc1017:23149–23389	+		23119	23469	91.7
	–		23389	23149	25.3
sc1017:23803–23901	+		23573	23991	92.6
	–		23943	23763	87.2
sc1018:68–470	+		68	470	6.2
	–		470	58	63.9
sc1018:39398–39759	+		39391	39759	81.8
	–	*NCS82*	39929	39398	98.1
sc1020:3716–4013	+		3716	4013	0.0
	–	*NCS71*	4116	3606	95.1
sc1020:4270–4488	+		4270	4488	52.1
	–		4568	4240	83.9
sc1020:22731–23586	+		22731	23616	71.8
	–		24306	22729	100.0
sc1020:52550–53355	+		52218	53355	90.8
	–		53355	52490	59.0
sc1020:54039–54241	+		53739	55041	100.0
	–		54241	54039	12.3
sc1020:54545–54748	+		53745	55041	100.0
	–		54748	54545	0.0
sc1020:54976–57752	+		54966	59245	72.9
	–	*NCS32*	57752	54956	75.3
sc1020:79835–80260	+		79795	80410	72.6
	–		80260	79835	5.9
sc1020:87293–87522	+		87253	87634	92.9
	–		87522	87293	10.9
sc1022:20893–21016	+		20443	21016	91.5
	–		22516	20881	100.0
sc1023:2454–2826	+		2434	2876	100.0
	–		2876	2454	29.3
sc1024:12371–12696	+		12261	12700	100.0
	–		12706	12341	31.7
sc1025:24448–24480	+		24348	24490	93.0
	–		24480	24448	78.8
sc1027:17084–17242	+		17044	17413	83.2
	–		17242	17084	31.4
sc1028:2027–2262	+		1269	2262	88.0
	–		2872	2027	91.4
sc1028:39441–39939	+		39441	39939	60.7
	–		39959	39188	98.3
sc1029:14930–15299	+	*NCS62*	14930	15459	96.0
	–		15299	14840	56.1
sc1029:26159–26356	+	*NCS54*	25899	26356	83.2
	–		27436	26151	100.0
sc1029:38296–38412	+		37995	38455	99.8
	–		39057	38286	99.3
sc1030:29320–30386	+	*NCS38*	29320	30446	55.2
	–		30386	29260	48.7
sc1031:35404–35604	+		35404	35604	49.8
	–		36286	35301	99.9
sc1033:24770–24913	+		24709	25354	100.0
	–		24963	24770	36.6
sc1033:49898–50136	+	*NCS83*	49888	50146	100.0
	–	*NCS75*	50502	49848	97.3
sc1034:1960–2116	+		1940	2116	75.1
	–		2168	1750	97.4
sc1034:37129–37556	+		37129	37556	0.0
	–		37678	37108	96.8
sc1036:59984–60178	+		59984	60178	0.0
	–		60508	59764	99.9

Continued on next page

Table S3, continued

Cluster coordinates	Inferred Precursor Transcript				
	Strand	Name	Start	End	Coverage (%)
sc1036:60993–61850	+		60993	61850	27.5
	–		61960	60747	100.0
sc1036:62937–63102	+		62122	63102	100.0
	–		64214	62937	97.7
sc1038:24981–25209	+		24891	25259	67.2
	–		25209	24981	52.8
sc1038:40735–41170	+		40735	41190	66.9
	–		41177	40347	99.9
sc1038:78785–78877	+		78524	78887	100.0
	–		80593	78785	99.2
sc1038:99617–99774	+		98328	99784	99.7
	–		100673	99617	99.0
sc1038:140777–140824	+		140757	140824	36.8
	–		140824	140767	6.3
sc1040:36238–36577	+	*NCS52*	36227	36660	99.1
	–		36577	36238	0.0
sc1040:37256–37420	+		37206	37490	84.2
	–		37420	37246	3.6
sc1040:123627–123701	+		122977	123721	100.0
	–		123711	123627	98.8
sc1040:180260–180348	+		180260	180348	55.1
	–		180350	180260	44.9
sc1040:195062–195337	+		195012	195337	61.3
	–		195337	195062	0.0
sc1041:89645–89736	+		88805	89746	100.0
	–		90562	89645	94.1
sc1041:101767–102804	+		101687	102814	100.0
	–		102814	101767	20.3
sc1043:4383–4807	+		3303	4892	99.9
	–		4807	4383	23.8
sc1043:14277–14528	+		14277	14538	21.0
	–		14528	14097	65.0
sc1043:45378–45481	+		45378	45602	82.6
	–		45481	45378	0.0
sc1043:45640–45767	+		45610	45807	94.4
	–		45767	45640	0.0
sc1044:46–774	+		26	784	97.2
	–	*NCS37*	874	46	65.3
sc1044:66037–66426	+		65601	66866	100.0
	–		66436	66037	18.8
sc1044:70189–71131	+		70189	71131	85.6
	–		71131	70139	42.9
sc1044:71474–71561	+		71414	71673	92.2
	–		71561	71474	28.4
sc1044:73216–73441	+		73216	73551	91.1
	–		73441	73216	11.1
sc1045:5356–5590	+		5186	6146	100.0
	–		5590	5316	27.3
sc1045:11221–11566	+		11221	11566	0.0
	–		12176	10471	100.0
sc1045:72660–72730	+		72090	72770	100.0
	–		72730	72660	69.0
sc1045:111842–111982	+		111842	111982	0.0
	–		111982	111842	0.0
sc1046:7429–7543	+		7179	7563	100.0
	–		7543	7429	41.7
sc1047:46135–46410	+		45041	46452	100.0
	–		47271	46135	90.9
sc1048:23852–24038	+	*NCS48*	23730	24042	100.0
	–		24038	23852	0.0
sc1050:34744–35601	+		34744	35601	2.9
	–	*NCS22*	35601	34714	86.8
sc1050:87452–87670	+		87452	87761	85.5
	–		87700	87452	20.1

Cluster coordinates	Inferred Precursor Transcript				
	Strand	Name	Start	End	Coverage (%)
sc1053:6186–6792	+		6186	6792	0.0
	–		6822	6146	69.1
sc1054:27472–27504	+	*NCS29*	27372	27524	98.0
	–		27504	27472	78.8
sc1055:50052–50551	+		50036	50551	84.1
	–		51125	50052	92.6
sc1055:78975–79463	+		78975	79463	17.8
	–		79521	78899	100.0
sc1055:81055–83050	+		81055	83050	36.7
	–	*NCS20*	83056	81055	99.6
sc1055:138817–138892	+		138387	138982	100.0
	–		138932	138777	79.5
sc1055:147036–147158	+	*NCS66*	146756	147370	97.4
	–		147158	147016	35.0
sc1055:156208–156447	+		156208	156447	10.4
	–		156447	156198	12.5
sc1055:158094–158319	+		157931	158761	98.9
	–		158319	158084	10.6
sc1055:162746–162961	+		162726	162973	85.4
	–		162961	162746	23.1
sc1056:17367–17625	+		16817	17825	96.2
	–		17695	17367	43.5
sc1056:31494–31606	+		29434	31606	100.0
	–		32656	31494	99.6
sc1056:145888–146432	+		145828	146432	26.7
	–		146457	145875	100.0
sc1056:165453–165750	+	*NCS18*	165443	165750	57.5
	–	*NCS7*	167232	165323	99.8
sc1056:166532–168895	+		166532	169001	88.0
	–	*NCS6*	168905	165322	96.0
sc1056:174775–174961	+		174035	174961	90.2
	–		175389	174775	99.5
sc1057:22742–23397	+		22712	23407	64.2
	–		23397	22102	93.4
sc1057:36897–37626	+		36897	37626	6.8
	–		37727	36797	66.7
sc1058:19613–20488	+		19613	20488	28.9
	–		20488	19613	12.0
sc1058:20682–21452	+		20682	21462	27.3
	–		21525	20551	90.4
sc1058:45831–46126	+		45226	46715	100.0
	–		46126	45831	0.0
sc1058:63376–63791	+		63376	63821	31.6
	–		63821	63366	95.2
sc1058:91631–92431	+		91541	92451	99.4
	–		93011	91611	90.8
sc1058:181315–181403	+		180232	181413	99.9
	–		182233	181295	99.7
sc1058:182450–182819	+		182440	182819	13.2
	–		183209	182368	99.9
sc1058:182991–183161	+		182991	183171	27.6
	–		183208	182368	100.0
sc1058:213594–214166	+		213574	214186	57.7
	–	*NCS56*	214266	213584	93.9
sc1059:25–2594	+		25	2594	77.5
	–		2607	15	81.9
sc1059:2851–3306	+		2851	3306	0.0
	–		3307	2571	91.3
sc1059:102338–102697	+		102306	102712	100.0
	–		102697	102338	0.0
sc1059:112648–112755	+		112418	112756	99.7
	–		112765	112648	75.0
sc1059:144909–146497	+		144909	146497	15.9
	–	*NCS12*	146507	144759	99.2

Cluster coordinates	Inferred Precursor Transcript				
	Strand	Name	Start	End	Coverage (%)
sc1060:25565–25673	+		24400	25673	98.5
	–		25993	25555	100.0
sc1060:39108–39165	+		38548	39200	100.0
	–		39751	39088	98.9
sc1060:42579–42718	+		42498	42721	100.0
	–		42976	42569	96.2
sc1060:52921–53199	+		52415	53199	94.7
	–		53199	52921	38.7
sc1061:40596–40933	+		40143	40933	100.0
	–		40943	40596	38.8
sc1061:41318–41547	+		41308	41547	10.4
	–		41567	40908	100.0
sc1061:133662–133857	+		133662	133867	4.1
	–		133917	132348	100.0
sc1063:2701–2992	+		1104	2992	93.4
	–	*NCS73*	3112	2701	96.0
sc1063:3222–3443	+		3202	3523	82.6
	–		3443	3222	22.5
sc1063:14927–15332	+		14927	15332	9.9
	–		15818	14827	100.0
sc1063:20875–20976	+		18455	21016	99.8
	–		21276	20875	86.3
sc1063:56615–56692	+		56605	56702	89.8
	–		56692	56615	32.1
sc1063:57039–57172	+		57019	57282	83.7
	–		57172	57039	18.7
sc1063:58684–58771	+		58624	58783	94.9
	–		58771	58684	28.4
sc2000:4199–4861	+		4147	4911	100.0
	–	*NCS63*	5631	4199	71.8
sc2000:53765–53901	+		53765	53901	18.2
	–		53901	53765	0.0
sc2000:86459–86528	+		86459	86742	87.5
	–		86528	86459	0.0
sc2000:90080–90252	+		90080	90258	42.5
	–		90258	90080	49.7
sc2001:3713–4119	+		3673	4149	41.7
	–	*NCS50*	4279	3643	68.1
sc2002:133190–133467	+		133020	135583	100.0
	–		133467	133190	0.0
sc2002:154632–154877	+		154626	154883	100.0
	–	*NCS78*	155142	154632	98.2
sc2003:115485–115693	+		115485	115733	30.1
	–		115693	115455	65.7
sc2003:132090–133685	+		131860	133862	99.7
	–		133715	132090	26.9
sc2003:135010–135312	+		134440	135332	100.0
	–		135312	135010	8.3
sc2003:144264–144336	+		143824	144357	100.0
	–		144449	144242	100.0
sc2003:227241–227476	+	*NCS46*	227221	227716	98.4
	–		227486	227241	39.8
sc2003:260941–261041	+		260491	261071	99.3
	–		262267	260881	99.9

Table S4. mRNA-Seq analysis of wild-type (WT) and RNAi-mutant strains. Each tag was comprised of the first 25 nt of a 36-nt Illumina read.

	WT_1	WT_2	Δ*ago1* _1	Δ*ago1* _2	Δ*dcr1* _1	Δ*dcr1* _2	Total
Sequencing							
Total reads (tags)	5,237,134	5,710,767	5,469,626	5,672,984	5,481,666	5,873,485	33,445,662
Unique tags	2,362,087	2,355,724	1,792,636	2,166,169	2,079,539	2,128,205	12,884,360
Mapping of tags							
Genome-matching tags	3,913,229	4,594,533	4,256,197	4,682,941	4,609,746	4,972,396	27,029,042
% of total tags	*74.7*	*80.5*	*77.8*	*82.5*	*84.1*	*84.7*	*80.8*
Unique genome-matching tags	1,239,480	1,439,462	905,718	1,367,051	1,367,339	1,416,775	7,735,825
% of total tags	*52.5*	*61.1*	*50.5*	*63.1*	*65.8*	*66.6*	*60.0*
Total genomic hits	1,283,574	1,487,146	943,739	1,415,491	1,415,527	1,467,372	8,012,849
Analysis							
rRNA tags	490,038	562,592	699,948	615,593	613,841	755,697	3,737,709
% of genome-matching tags	*12.5*	*12.2*	*16.4*	*13.1*	*13.3*	*15.2*	*13.8*
tRNA tags	559	566	738	604	576	722	3,765
% of genome-matching tags	*<0.1*	*<0.1*	*<0.1*	*<0.1*	*<0.1*	*<0.1*	*<0.1*
Sense annotated ORF tags	2,949,357	3,426,898	3,167,181	3,518,675	3,487,311	3,705,506	20,254,928
% of genome-matching tags	*75.4*	*74.6*	*74.4*	*75.1*	*75.7*	*74.5*	*74.9*
Antisense annotated ORF tags	74,307	84,847	102,596	92,149	94,662	115,526	564,087
% of genome-matching tags	*1.9*	*1.8*	*2.4*	*2.0*	*2.1*	*2.3*	*2.1*

Table S6. Number of colonies obtained upon transformation of each strain with the plasmid indicated, labeled as in figure S11A. Three independent transformations are shown (summed in figure S11A).

Plasmid	Transformation 1			Transformation 2			Transformation 3		
	WT	Δ*ago1*	Δ*dcr1*	WT	Δ*ago1*	Δ*dcr1*	WT	Δ*ago1*	Δ*dcr1*
CEN	66	0	0	186	5	8	48	0	2
2μ	77	9	6	10	0	1	18	2	0
2μ Ago1	106	5	20	98	0	0	21	2	5
2μ Ago1, induced	68	44	3	78	26	0	23	26	1
2μ Dcr1	95	9	4	51	0	3	23	0	4
2μ Dcr1, induced	58	2	70	48	0	24	36	0	33

Table S7. Strains used and generated in this study.

Strain	Genotype	Species	Reference
FY45	*MAT***a**/*MAT* α	*S. cerevisiae* S288C	(*30*)
F2035	*MAT***a**/*MAT* α	*S. bayanus* MCYC623	NCYC
KpolWT	Wild-type	*K. polysporus* DSM70294	(*31*)
Can14	*MAT***a**/*MAT* α	*C. albicans* SC5314	(*32*)
F2037	Wild-type	*S. castellii* CBS4309	NCYC
Y235	*MAT***a**/*MAT* α *ura3-1/ura3-1*	*S. castellii* CBS4310	(*33*)
DPB002	*MAT***a**/*MAT* α *ura3-1/ura3-1 ago1*Δ*::HYG/ago1*Δ*::HYG*	*S. castellii* CBS4310	This study
DPB003	*MAT***a**/*MAT* α *ura3-1/ura3-1 dcr1*Δ*::loxP-KanMX6-loxP/dcr1*Δ*::loxP-KanMX6-loxP*	*S. castellii* CBS4310	This study
DPB004	*MAT***a** *ura3-1 ho*Δ	*S. castellii* CBS4310	This study
DPB006	*MAT***a** *ura3-1 ho*Δ *ago1*Δ*::HYG*	*S. castellii* CBS4310	This study
DPB008	*MAT***a** *ura3-1 ho*Δ *dcr1*Δ*::loxP-KanMX6-loxP*	*S. castellii* CBS4310	This study
DPB005	*MAT* α *ura3-1 ho*Δ	*S. castellii* CBS4310	This study
DPB007	*MAT* α *ura3-1 ho*Δ *ago1*Δ*::HYG*	*S. castellii* CBS4310	This study
DPB009	*MAT* α *ura3-1 ho*Δ *dcr1*Δ*::loxP-KanMX6-loxP*	*S. castellii* CBS4310	This study
DPB220	*MAT* α *ura3-1 ho*Δ *Flag*$_3$*-AGO1*	*S. castellii* CBS4310	This study
DPB313	*MAT* α *ura3-1 ho*Δ *ago1*Δ*::HYG*	*S. castellii* CBS4310	This study
DPB318	*MAT* α *ura3-1 ho*Δ *dcr1*Δ	*S. castellii* CBS4310	This study
DPB314	*MAT* α *ho*Δ *ura3::EGFP(S65T)-KanMX6*	*S. castellii* CBS4310	This study
DPB317	*MAT* α *ho*Δ *ago1*Δ*::HYG ura3::EGFP(S65T)-KanMX6*	*S. castellii* CBS4310	This study
DPB321	*MAT* α *ho*Δ *dcr1*Δ *ura3::EGFP(S65T)-KanMX6*	*S. castellii* CBS4310	This study
DPB331	*MAT* α *ho*Δ *ura3::EGFP(S65T)-KanMX6 c633::plp*	*S. castellii* CBS4310	This study
DPB332	*MAT* α *ho*Δ *ura3::EGFP(S65T)-KanMX6 c633::plp-weakSC_GFP*	*S. castellii* CBS4310	This study
DPB333	*MAT* α *ho*Δ *ura3::EGFP(S65T)-KanMX6 c633::plp-strongSC_GFP*	*S. castellii* CBS4310	This study
DPB334	*MAT* α *ho*Δ *ago1*Δ*::HYG ura3::EGFP(S65T)-KanMX6 c633::plp*	*S. castellii* CBS4310	This study
DPB335	*MAT* α *ho*Δ *ago1*Δ*::HYG ura3::EGFP(S65T)-KanMX6 c633::plp-weakSC_GFP*	*S. castellii* CBS4310	This study
DPB336	*MAT* α *ho*Δ *ago1*Δ*::HYG ura3::EGFP(S65T)-KanMX6 c633::plp-strongSC_GFP*	*S. castellii* CBS4310	This study
DPB337	*MAT* α *ho*Δ *dcr1*Δ *ura3::EGFP(S65T)-KanMX6 c633::plp*	*S. castellii* CBS4310	This study
DPB338	*MAT* α *ho*Δ *dcr1*Δ *ura3::EGFP(S65T)-KanMX6 c633::plp-weakSC_GFP*	*S. castellii* CBS4310	This study
DPB339	*MAT* α *ho*Δ *dcr1*Δ *ura3::EGFP(S65T)-KanMX6 c633::plp-strongSC_GFP*	*S. castellii* CBS4310	This study
F2005	*MAT* α *his3*Δ*1 leu2*Δ*0 lys2*Δ*0 ura3*Δ*0*	*S. cerevisiae* BY4742	(*30*)
L4718	*MAT* α *leu2-3,112 trp1-1 can1-100 ura3-1 ade2-1 his3-11,15*	*S. cerevisiae* W303-1B	(*34*)
DPB249	*MAT* α *leu2-3,112 trp1-1 can1-100 ura3::EGFP(S65T)-KanMX6 ade2-1 his3-11,15*	*S. cerevisiae* W303-1B	This study
DPB250	*MAT* α *leu2-3,112 trp1-1 can1-100 ura3::EGFP(S65T)-KanMX6 ade2-1 HIS3::pGAL1-weakSC_GFP*	*S. cerevisiae* W303-1B	This study
DPB251	*MAT* α *leu2-3,112 trp1-1 can1-100 ura3::EGFP(S65T)-KanMX6 ade2-1 HIS3::pGAL1-strongSC_GFP*	*S. cerevisiae* W303-1B	This study
DPB255	*MAT* α *LEU2::pTEF-Dcr1 trp1-1 can1-100 ura3::EGFP(S65T)-KanMX6 ade2-1 his3-11,15*	*S. cerevisiae* W303-1B	This study
DPB256	*MAT* α *LEU2::pTEF-Dcr1 trp1-1 can1-100 ura3::EGFP(S65T)-KanMX6 ade2-1 HIS3::pGAL1-weakSC_GFP*	*S. cerevisiae* W303-1B	This study
DPB257	*MAT* α *LEU2::pTEF-Dcr1 trp1-1 can1-100 ura3::EGFP(S65T)-KanMX6 ade2-1 HIS3::pGAL1-strongSC_GFP*	*S. cerevisiae* W303-1B	This study
DPB258	*MAT* α *LEU2::pTEF-Dcr1 TRP1::pTEF-Ago1 can1-100 ura3::EGFP(S65T)-KanMX6 ade2-1 his3-11,15*	*S. cerevisiae* W303-1B	This study
DPB259	*MAT* α *LEU2::pTEF-Dcr1 TRP1::pTEF-Ago1 can1-100 ura3::EGFP(S65T)-KanMX6 ade2-1 HIS3::pGAL1-weakSC_GFP*	*S. cerevisiae* W303-1B	This study
DPB260	*MAT* α *LEU2::pTEF-Dcr1 TRP1::pTEF-Ago1 can1-100 ura3::EGFP(S65T)-KanMX6 ade2-1 HIS3::pGAL1-strongSC_GFP*	*S. cerevisiae* W303-1B	This study
DPB271	*MAT* α *leu2-3,112 trp1-1 can1-100 ade2-1 his3-11,15*	*S. cerevisiae* W303-1B	This study
DPB272	*MAT* α *leu2-3,112 trp1-1 can1-100 ade2-1 HIS3::pGAL1-hpSC_URA3*	*S. cerevisiae* W303-1B	This study
DPB275	*MAT* α *LEU2::pTEF-Dcr1 TRP1::pTEF-Ago1 can1-100 ade2-1 his3-11,15*	*S. cerevisiae* W303-1B	This study
DPB276	*MAT* α *LEU2::pTEF-Dcr1 TRP1::pTEF-Ago1 can1-100 ade2-1 HIS3::pGAL1-hpSC_URA3*	*S. cerevisiae* W303-1B	This study

Table S8. Plasmids generated in this study.

Plasmid	Description
pYES2.1-Ago1	2-micron plasmid, *S. castellii AGO1* under *GAL1* promoter
pYES2.1-Dcr1	2-micron plasmid, *S. castellii DCR1* under *GAL1* promoter
pYES2.1-GFP	2-micron plasmid, *GFP* under *GAL1* promoter
pET101-Dcr1	*E. coli* Dcr1 expression plasmid
pIp	*S. castellii* integrating plasmid, empty
pIp-weakSC_GFP	*S. castellii* integrating plasmid, weak *GFP* silencing construct under *S. cerevisiae GAL1* promoter
pIp-strongSC_GFP	*S. castellii* integrating plasmid, strong *GFP* silencing construct under *S. cerevisiae GAL1* promoter
pRS404-P_{TEF}-Ago1	*S. cerevisiae* integrating plasmid, *S. castellii AGO1* under *TEF* promoter
pRS405-P_{TEF}-Dcr1	*S. cerevisiae* integrating plasmid, *S. castellii DCR1* under *TEF* promoter
pRS403-P_{GAL1}-weakSC_GFP	*S. cerevisiae* integrating plasmid, weak *GFP* silencing construct under *GAL1* promoter
pRS403-P_{GAL1}-strongSC_GFP	*S. cerevisiae* integrating plasmid, strong *GFP* silencing construct under *GAL1* promoter
pRS403-P_{GAL1}-hpSC_URA3	*S. cerevisiae* integrating plasmid, hairpin *URA3* silencing construct under *GAL1* promoter

Supplemental References

S1. E. Astromskas, M. Cohn, *Yeast* **24**, 499 (2007).
S2. U. Guldener, S. Heck, T. Fielder, J. Beinhauer, J. H. Hegemann, *Nucleic Acids Res* **24**, 2519 (1996).
S3. M. D. Krawchuk, W. P. Wahls, *Yeast* **15**, 1419 (1999).
S4. A. L. Goldstein, J. H. McCusker, *Yeast* **15**, 1541 (1999).
S5. M. S. Longtine *et al.*, *Yeast* **14**, 953 (1998).
S6. R. D. Gietz, R. H. Schiestl, *Nat Protoc* **2**, 31 (2007).
S7. A. Sigova, N. Rhind, P. D. Zamore, *Genes Dev* **18**, 2359 (2004).
S8. D. Mumberg, R. Muller, M. Funk, *Gene* **156**, 119 (1995).
S9. R. S. Sikorski, P. Hieter, *Genetics* **122**, 19 (1989).
S10. G. S. Pall, C. Codony-Servat, J. Byrne, L. Ritchie, A. Hamilton, *Nucleic Acids Res* **35**, e60 (2007).
S11. C. S. Hoffman, F. Winston, *Gene* **57**, 267 (1987).
S12. D. J. Garfinkel, M. F. Mastrangelo, N. J. Sanders, B. K. Shafer, J. N. Strathern, *Genetics* **120**, 95 (1988).
S13. M. J. Curcio, D. J. Garfinkel, *Proc Natl Acad Sci U S A* **88**, 936 (1991).
S14. S. E. Adams *et al.*, *Cell* **49**, 111 (1987).
S15. S. D. Youngren, J. D. Boeke, N. J. Sanders, D. J. Garfinkel, *Mol Cell Biol* **8**, 1421 (1988).
S16. A. Grimson *et al.*, *Nature* **455**, 1193 (2008).
S17. J. L. Gordon, K. P. Byrne, K. H. Wolfe, *PLoS Genet* **5**, e1000485 (2009).
S18. C. Neuveglise, H. Feldmann, E. Bon, C. Gaillardin, S. Casaregola, *Genome Res* **12**, 930 (2002).
S19. C. Llorens, R. Futami, D. Bezemer, A. Moya, *Nucleic Acids Res* **36**, D38 (2008).
S20. E. R. Havecker, X. Gao, D. F. Voytas, *Genome Biol* **5**, 225 (2004).
S21. Y. Gelfand, A. Rodriguez, G. Benson, *Nucleic Acids Res* **35**, D80 (2007).
S22. J. Schultz, F. Milpetz, P. Bork, C. P. Ponting, *Proc Natl Acad Sci U S A* **95**, 5857 (1998).
S23. I. Letunic, T. Doerks, P. Bork, *Nucleic Acids Res* **37**, D229 (2009).
S24. C. Notredame, D. G. Higgins, J. Heringa, *J Mol Biol* **302**, 205 (2000).
S25. J. Soding, A. Biegert, A. N. Lupas, *Nucleic Acids Res* **33**, W244 (2005).
S26. N. T. Ingolia, S. Ghaemmaghami, J. R. Newman, J. S. Weissman, *Science* **324**, 218 (2009).
S27. U. Nagalakshmi *et al.*, *Science* **320**, 1344 (2008).
S28. J. Houseley, K. Kotovic, A. El Hage, D. Tollervey, *Embo J* **26**, 4996 (2007).
S29. T. J. Goodwin, D. E. Dalle Nogare, M. I. Butler, R. T. Poulter, *Yeast* **20**, 493 (2003).
S30. C. B. Brachmann *et al.*, *Yeast* **14**, 115 (1998).
S31. D. R. Scannell *et al.*, *Proc Natl Acad Sci U S A* **104**, 8397 (2007).
S32. W. A. Fonzi, M. Y. Irwin, *Genetics* **134**, 717 (1993).
S33. R. F. Petersen *et al.*, *J Mol Biol* **318**, 627 (2002).
S34. B. J. Thomas, R. Rothstein, *Cell* **56**, 619 (1989).